Optimal Formation Flight Control Using Coupled Inter-Spacecraft Dynamics

Martin Azkarate Vecilla

September 2009

Optimal Formation Flight Control Using Coupled Inter-Spacecraft Dynamics

by Martin Azkarate Vecilla

Research realized at the Space Systems Laboratory (Massachusetts Institute of Technology, Cambridge, USA) and submitted to Institut Supérieure de l'Aéronautique et de l'Espace (SUPAERO, Toulouse, FRANCE) and to Telecom BCN (Barcelone, Spain) on September 28, 2009 in partial fulfillment of the requirements for the Double Degree of Master of Science *Ingénieur SUPAERO - Enginyer Superior de Telecomunicació (ETSETB, UPC, Barcelona)* and for the *Master de Recherche SAID* from École Doctorale Systèmes, Toulouse, FRANCE

Abstract

The increasing number of formation flight space missions proposed by the scientific community for the near future has led many researchers to the study, development and implementation of optimal control systems applied to a multi-spacecraft system. The approaches taken may vary among authors, but it is generally agreed upon that having independent controllers at each spacecraft leads to a non-optimal solution in a global or formation-wide sense, even when independent controllers are implemented using any of the locally optimal techniques known from the theory of control. Most of the future formation flight missions have been designed with an interferometric purpose, such as performing a space-based distributed telescope structure that would fly into deep space with an observational objective. In that case, where global positioning systems such as GPS are no longer available, relative positioning not only becomes necessary to achieve control of the multi-spacecraft system, but it also becomes a crucial factor that would determine the performance of the system with regards to the optical science output. In fact, if we redefine the state vector of the plant and use the relative states that need to be tracked instead of independent global positions, we get to a definition with coupled dynamics of the whole multi-agent system.

This research focuses on the control performance obtained when the controller is designed using coupled inter-spacecraft dynamics and how this approach can lead to an optimal solution in a global sense, both in optical performance and overall fuel usage. The first part of the thesis will address the theoretical advantages that may arise within the coupled dynamics architecture and the second part analyses the performance of the results obtained when testing the real implementation of the controller on hardware. This study, concerning implementation and performance of formation flight controllers in a real case scenario such as deep space interferometer missions, will lead towards increasing mission lifetime, performance improvement and a step forward in the field.

Acknowledgments

I would like to thank Telecom BCN (Universitat Poltecnica de Catalunya) for the great education provided and for opening my academic career path. Thanks also to Institute Superieure de l'Aeronautique et de l'Espace (SUPAERO) for the excellent training and for being so helpful. Especial thanks to Professors Caroline Berard, Daniel Alazard, Karen Thompson and Dr. Frédéric Dehais for their help and support.

I wish to express my gratitude to MIT and especially to the Space Systems Laboratory for letting me conduct this research within their lab. Especial thanks are given to Professor Dave Miller, Dr. Alvar Saenz-Otero and to the Spheres Team for their support and guidance. Working next to you was an impresive experience.

Thanks to the Anardinar Team for making of daily life in Boston such a great experience.

Thanks to the AST Team for all the expriences shared within the two years in Supaero.

Thanks to my friends in Barcelona and Donostia for making me feel unique and special.

And finally, thanks to my girlfriend and my family for their continous support, all my love for them.

Contents

List of Figures

List of Tables

Chapter 1

Introduction

1.1 Motivation

In human beings' intrinsic behaviour, within our natural instinct of curiosity, lies the need for conquering new areas, places or fields of space. Not satisfied enough with the discovery of new continents, humans have always needed to extend their arms towards another direction, towards another dimension. It was not until the first flight of the history made by the Wright brothers that the door opened in the "z" vertical direction. People thought that humans would eventually reach the sky, but in fact, when the Russians opened the star gate in 1957, they showed the world that there are no limits in the sky, nor in this reference frame called the universe.

And since that day a new burst of passion has kept the scientific community fascinated and captivated each and every time that a new planet is discovered, a Pathfinder reaches Mars or an Automated Transfer Vehicle docks with the International Space Station.

Since the first launch of a satellite into the space, spatial technology has developed highly. This has enabled huge advances into the laborious task of conquering the vast outer space. In spite of the fact that humans have contemplated the "ceiling" above them for centuries, it was due to the latest progress in several observation techniques and interferometer technology that we now can observe, with higher quality and precision, stars and planets so far away from the Earth, even those from external

galaxies.

It is important to mention that satellites have played a principal and leading role here, as they have provided a new means of observation. Circumventing attenuation, added noise and distortion that different layers of the atmosphere produce to the received signal, space-based telescopes have become an emerging technology in recent decades providing resolutions that are inconceivable for any ground-based telescope. The Hubble Space Telescope [14], for example, whose aperture diameter exceeds 2m, made pictures available of the most remote observed objects in the universe. There exists, however, a limitation in the resolution that a space-based monolith telescope can give due to the relationship between the image quality and the aperture diameter and the fact that these telescopes must fit within the confines of a space launcher.

The physical limitation can be overcome by means of a distributed telescope structure. The same technology that is used in the ground-based telescope array systems can be carried to the space and use a network of collectors to constructively combine the light coming from a further point in the space. The angular resolution improvement that such a formation of satellites can provide is very encouraging.

Furthermore, there are multiple benefits of a distributed space system. System reliability, redundancy, reconfigurability and modularity apart from the aforementioned angular resolution are probably the most valuable advantages that formation flying space systems allow. Taking these advantages into consideration some future observation missions have already been designed, such as ESA's DARWIN mission [22] or NASA's Terrestrial Planet Finder (TPF) [25] both of them thought to detect Earth-like planets orbiting nearby stars, and search for evidence of life.

The scientific output of these missions will depend on the best achievable image quality. It is known that the angular resolution of an interferometer is dependent on the location of different apertures [1] and more precisely, the baselines separating them. The capability of collecting light from the same source at different precise baselines will determine the performance of the distributed telescope. Controlled reconfigurations in the relative positioning of the formation will enable the different baselines to be covered. However, the interferometric techniques require these base-

lines to be tracked within a very narrow error margin. The positioning control of the multi-spacecraft system would be a key milestone of this new challenging technology. Thus, the purpose of this research is to design and implement a control system that fulfills these requirements.

1.2 Literature Review

The beginning of distributed space telescope technology promoted the research of formation flying algorithms. Several authors have worked on the design of controllers for a multi-agent system and publications explaining the different approaches taken are multiple. Most of them would agree that using staged control is a suitable high-level approach, where initially a roughly controlled formation configuration is achieved using wide-range low-precision actuators and finally a precise control of the formation is assured by means of narrow range but higher precision actuators. The strategies followed by the authors may differ at the precise control stage level.

For the present study an extensive literature review has been considered necessary for the better understanding of the strategies that have been used in the past by several authors and that are the state of the art in formation flight algorithms. Different approaches may be grouped into four formation flight control architectures [8],[7]:

- Leader-Follower
- Cyclic
- Multi-Input Multi-Output
- Virtual Structure

Leader-Follower architecture is surely the most studied one. In this architecture, individual spacecraft controllers are connected hierarchically reducing the formation control to individual tracking problems. Stability of this control architecture is usually demonstrated ([39],[38]) using *control dependency directed graphs* which is based

on the prior automated highway system (AHS) literature. Most of the work done in the Leader-Follower architecture field differ in the control strategy or technique used for the follower's control law. Adaptative [12], feedback linearized [30], [41], model predictive with linear time-varying models [23], non-linear [28] and robust [11] techniques among others have already been used within the Leader-Follower architecture. The main issue of this architecture is found on the propagation, towards the followers, of the disturbances felt by the leaders and guaranteeing that these do not increase as we go down in the hierarchic line (mesh stability).

Cyclic architecture, which could be considered a particular case of the previous one, does a non-hierarchical connection between the controllers, leading to a *cyclic control dependency directed graph.* Cyclic algorithms rely on the stability convergence of the controllers and result in different formation moving shapes. Important work in this field can be found in [26], [15].

MIMO architecture defines a dynamic model of the entire formation, considering it as a whole multi-input multi-output plant. Under this consideration the theory of control can be applied as in any other individual system although global stability of the formation is already assured. Most advanced and important work concerning formation control using MIMO architecture is done by Dr. Roy Smith and Dr. Fred Hadaegh [35], [36], [37].

In the Virtual Structure architecture, the formation behaves like a virtual rigid body whose motion is used to generate reference trajectories for spacecrafts that will lately be tracked with individual controllers. Very interesting work is done in [24], where a formation template (i.e. virtual structure) is computed at each time step where a virtual center of a formation is considered through a LS (Least-Squares) fit and minimizes the tracking error of the whole formation.

On the other hand, a thorough research has been conducted on the subject of implementation of formation flying algorithms for the SPHERES testbed at MIT as well as for the International Space Station, which is the place where the real science occurs. The most important references related to this topic are Dr. Alvar Saenz-Otero thesis [33], [34], Mark Hilstad thesis [13] and Dr. Simon Nolet thesis

[29] thesis, concerning the theoretical development of the testbed and some internal documents showing how to interact with the software architecture and code new algorithms [27], [32]. Moreover, a big amount of publications by several members of the SPHERES Team helped in a better comprehension of formation flight algorithms design and posterior realization in the testbed. Main results of the research conducted by the SPHERES Team can be found in [3], [6], [2] as well as in the recently renewed SPHERES ISS Data Base website [40].

An important reference needs to be done to the optimal control books [21], [19] that have been a common reference throughout this thesis, as well as [18] for nonlinear control systems.

The research performed in this present thesis concerns the development of new formation flight controllers applied for the SPHERES testbed to optimally fulfill the control requirements of a distributed space telescope structure.

1.3 SPHERES Testbed

Synchronized Position Hold, Engage, Re-orient, Experimental Satellites (SPHERES) was thought and designed to offer scientists a testing environment where iteratively could develop algorithms of guidance, navigation and control (GN&C) for distributed spacecraft systems in microgravity scenarios. With a high test reliability and reproducibility, the SPHERES testbed allows the scientist to carry out research in algorithms in a risk-tolerant environment, enabling a low-cost maturation process.

With the collaboration of NASA the SPHERES Team at the Space Systems Laboratory (SSL, MIT) develops estimation, command and autonomy algorithms for formation flight space systems in order to get the technology of distributed satellites to a mature point so it can be exploited in future space missions. The SPHERES project needed to have at its disposal a testing tool where microgravity scenarios could be reproduced with a high reliability of the obtained resultant data so that the computed algorithms could be validated for reel use. Only that way the control techniques could be iteratively developed in efforts to get the architecture ready to

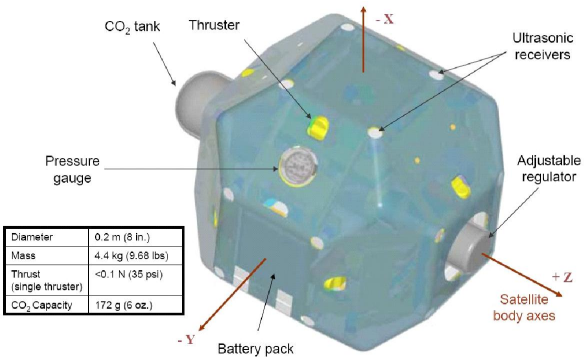

Figure 1.1: A SPHERE satellite

work on reel conditions. The risk-tolerant property is essential for its evolution so still-not-validated algorithms can be tested without damaging the system -no matter how aggressive the algorithms are- and for the lowest possible cost.

1.3.1 Main Characteristics

The SPHERES testbed consists of three free-flyer vehicles (commonly referred to as "satellites" or "spheres"), five ultrasonic beacons, and a laptop control station. The satellites are equipped in order to be self-contained during a flight test and have all the main functionalities of a satellite.

• The power supply is achieved with boarded batteries that can be recharged when they empty.

• The propulsion subsystem comprises 12 cold-gas thrusters fed by a tank containing liquid CO2 propellant, also with the possibility of replacement and recharge. Variable forces and torques can be produced using pulse modulation with a minimum time resolution of one millisecond.

• Communication is provided by a RF link with two frequency channels, one for communication between satellites (STS) and another for communication between satellite and laptop (STL). The second one is used for command sending and test data storage.

• Infra-red and ultrasonic sensors and emitters are used by the global positioning subsystem. This one makes range measurements using the time of flight of the signal

emitted by the five beacons located at precisely known positions on the laboratory reference frame. Inertial data is also obtained by the IMU at a higher frequency than the external one using measurements of accelerometers and gyroscopes. This will allow the determination of position and attitude of the 3 spheres on global and local frames.

• The external control panel is reduced and simple as interaction between human-machine is done via the laptop control interface.

• Flight software coded in C is downloaded to a Texas Instrument DSP that will run the algorithms. Standard electronic devices (samplers, controllers, UART, etc) are also included in the hardware of the spheres.

• The software has both periodic interrupt functions and event-driven task functions to implement control and estimation algorithms with elevated freedom. Most of the parameters of those functions such as the interruption period or event-mask can be reconfigured as preferred.

Finally, the SPHERES Guest Scientists Program provides the scientists with documentation that details the interfaces to the existing flight code in order to implement custom algorithms. A Matlab simulation that models the dynamics of the satellites with a double integrator plant will initially serve for the debugging of the code.

1.3.2 Air table Tests

Once that custom code is debugged using simulation tools and their performances acquire the specifications in demand of scientists the next step in the validation of the algorithm happens while testing in the hardware, in the spheres. As it could be expected, the algorithms are designed to be used in a 0-g environment, so in order to get closer to microgravity dynamics the SSL has built an air table in the laboratory that fakes zero-gravity for the cost of loosing one space dimension. The air table makes the spheres float, within a very thin air layer, which keeps its altitude constant (loss of vertical dimension) and reducing the free-motion to 2D (horizontal plan) in return. Consequently, the number of degrees-of-liberty (DOL) for an air table test is reduced to 3 (two for horizontal translation, one for attitude), instead of the 6 DOL

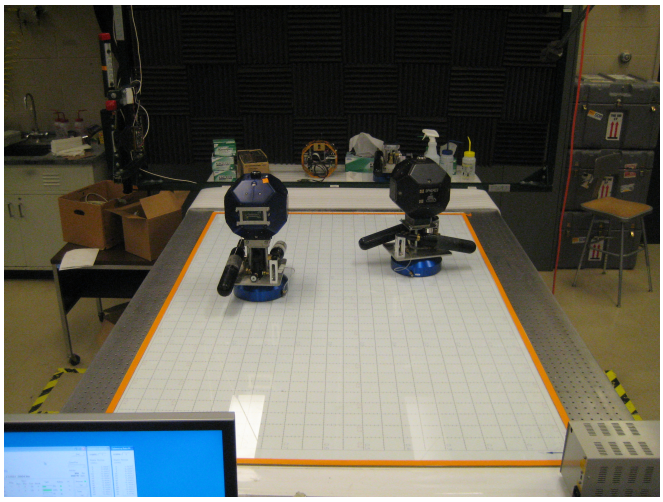

Figure 1.2: Air table test

motion that we would usually desire to test. Nevertheless, the collected data at air table tests serves to validate algorithms in the reel hardware. The fact that all parts of the system –propulsion and communication subsystems, inertia and dynamics, etc- are not mathematically modelled anymore when testing on hardware permits a much more realistic evaluation of the output data and performance of the custom algorithm.

1.3.3 Testing at zero-gravity environment

The final validation of the algorithm takes place in space, inside the International Space Station (ISS), where reel zero-gravity environment is given. Astronauts at the ISS have permanently available a SPHERES testbed, with three satellites, five ultrasonic beacons and the laptop control station. A test session at the ISS laboratories needs organization and preplanning in advance –at the moment a total of 19 test sessions have been run at the ISS, with an approximate mean duration of 3 to 4 hours for each test session– so only the algorithms that have proved their good operability at the air table are valid to be tested at the ISS. The chosen ones will be transferred by NASA to the ISS. At the beginning of the test session, the astronauts will load the code in the spheres and will launch the tests from the laptop control station interface

Figure 1.3: International Space Station (ISS) test

using the procedures documentation provided by the SPHERES Team that details the steps to follow to get valid data.

The algorithms that show working operability close to the expected performance may eventually be validated for use in future multi-spacecraft space missions where the reel environment conditions are similar to those of the test.

1.4 Thesis Objectives

The main objective of the thesis is the design and implementation of optimal formation flight controllers that could be applied to interferometric space missions. Optimality will be searched to track the requested baselines for imaging maneuvers while a reduced use of available resources is made. In this thesis a new architecture for the control of the SPHERES multi-agent system is proposed. The innovation is found in the use of coupled inter-spacecraft dynamics that are defined when introducing into the state vector of the system the relative states –position and velocity- connecting the members of the flotilla. A complete design and analysis of the architecture will be made and the advantages that it reveals will be presented. The architecture will be further used for the implementation of optimal controllers. In order to evaluate the performance improvement that the architecture can provide several common scenar-

ios of interferometric maneuvers in real space missions will be presented. Controllers defining coupled dynamics will be tested in those scenarios and their performance will be compared to the one obtained by other controllers that do not use the coupled dynamics architecture. The worthiness of using a controller with coupled dynamics will also be evaluated, as the improvement in performance will be balanced against the drawbacks that this kind of architecture presents. Finally, this study will contribute in the science goal of the development of deep space formation flight controllers as it is prevented from using telemetry data from any global positioning system.

1.5 Thesis Outline

Following the line of the thesis objectives, chapter 2 focuses on the analysis of the architecture characteristics that uses coupled inter-spacecraft dynamics. The approach towards the search of optimality followed by the author and that led to the initial design of the architecture is also presented. The advantages that can be deemed from that architecture are discussed along the chapter. The following chapter introduces the selected scenarios where the architecture is willing to be tested as well as the other architectures to be compared to. The scientific requirements of each scenario will serve to define different cost functions. The latest ones will be used for the implementation of optimal controllers within the coupled dynamics architecture, as the cost functions will determine the criteria to minimize in the optimal control problem. At the end of chapter 3 the results obtained from testing the controllers in the SPHERES testbed are presented and the performance improvement when compared to other architectures is discussed. Chapter 4 focuses on the disadvantages of using coupled dynamics on the design of a formation flight control system. It also provides solutions that may reduce the effect of these drawbacks. Particular tests will be run to demonstrate the capability of the control system to operate under non-nominal circumstances where these disadvantages are more noticeable. An evaluation of the performance obtained in non-nominal cases is done at the end of the chapter. In the 5th and last chapter the most important conclusions of the previous chapters are col-

lected and the overall worthiness of the coupled dynamics architecture is evaluated. Finally, possible future work is proposed in order to keep on working on maturation process of optimal formation flight controllers.

Chapter 2

Coupled Dynamics Architecture

2.1 Searching Optimality

The main application of formation flying space systems is the creation of a distributed sensors structure that allows observation of further celestial objects with an increased angular resolution. The interferometer techniques lying on the basis of this space-based distributed telescope structure require a precise formation control, while accuracy in relative positioning becomes vital for the observational scientific output.

On the other hand, in deep space scenario, where most of the current formation flight space missions in development are placed, no accurate global positioning system is available, and so, using relative sensing among the members of the fleet becomes necessary for the formation control.

It is worth mentioning that under these circumstances the global inertial position of the satellites is mostly irrelevant as long as the global trajectory of the fleet is roughly controlled.

Bearing these ideas in mind, a formation flight controller is willing to be designed that will optimally track the relative states –position and velocity– between satellites. The controller should be able to track any formation shape and should require the less possible human interaction in order to achieve autonomous reconfiguration capability.

It must be noticed that this controller has a formation-wide objective to accomplish such as the one of tracking all the relative states among satellites and not just

the tracking of inertial position of one independent satellite. In order to approach this problem in an optimal way the following assumption has been made. Information of the states of other satellites –wether this are global or relative– is needed and the control commands must be computed taking those states into account. However, no hierarchic levels through the members of the fleet will be recognized due to the poor disturbance rejection properties of the Leader-Follower architecture mentioned before and the undesirable over-reliance on one satellite.

Then, supposing that each satellite is able to get within the control loop period the current relative states to the other satellites, the control commands can be performed depending on the actual error on those instead of being a function of the error in global independent positions which is the case of most of the formation flight controllers implemented up to the moment.

This approach may lead us to a redefinition of the system state vector which will not comprise global states of satellites anymore but will instead comprise the relative states of the whole formation. For example, the redefinition of the state vector for a three satellite formation would be:

Using global states we had:

$$\begin{aligned} x_{sat} &= [pos, vel] \equiv global\ states\ for\ a\ single\ satellite \\ x_{for} &= [x_{sat1}, x_{sat2}, x_{sat3}] \equiv state\ vector\ of\ the\ whole\ formation\ system \end{aligned} \tag{2.1}$$

Using relative states we have:

$$x_{for} = [p_{rel12}, v_{rel12}, p_{rel23}, v_{rel23}, p_{rel31}, v_{rel31}] \tag{2.2}$$

Note: p_{relij} and v_{relij} are the relative position and velocity states defined as from satellite i to satellite j

It must be noticed that the relative vectors in the formation state vector are defined in the inertial frame, and not in local body frame for each satellite, as the global attitude of each satellite is supposed to be controlled by means of star-trackers

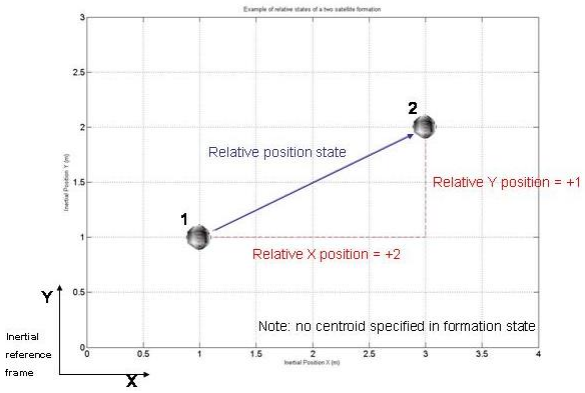

Figure 2.1: Example of relative state definition

or other attitude sensors. From now on, the global attitude will be assumed to be controlled decentralized –the personal implementation does control the attitude of satellites– but it will not be part of the future discussion as only the performance in relative positioning will be analyzed.

Figure 2.1 shows an example of how relative states between satellites should be defined. Note that for this example only position states have been defined and that as vectors in the inertial frame they have a determined direction and therefore these are signed.

Linearized dynamic equations using the redefined state vector must be rewritten for each of the axes (1D) of the inertial frame, as follows:

$$\begin{aligned} \dot{x}_{for} &= Ax_{for} + Bu \\ y &= Cx_{for} \end{aligned} \tag{2.3}$$

Where u contains the force actuators of each of the satellites put together in a column vector. A matrix corresponds to the common double integrator dynamics matrix, augmented to the number of existing relative vectors depending on the members of the formation. C matrix is the identity matrix with same size as A. And B becomes:

$$A = \begin{bmatrix} 0 & 1 & 0 & 0 & 0 & 0 \\ 0 & 0 & 0 & 0 & 0 & 0 \\ 0 & 0 & 0 & 1 & 0 & 0 \\ 0 & 0 & 0 & 0 & 0 & 0 \\ 0 & 0 & 0 & 0 & 0 & 1 \\ 0 & 0 & 0 & 0 & 0 & 0 \end{bmatrix}$$

$$B = \frac{1}{m} \begin{bmatrix} 0 & 0 & 0 \\ -1 & 1 & 0 \\ 0 & 0 & 0 \\ 0 & -1 & 1 \\ 0 & 0 & 0 \\ 1 & 0 & -1 \end{bmatrix} \tag{2.4}$$

where m is the mass of a single satellite.

We can easily see now that this redefinition of the state vector has led us to some equations that show dynamics with coupled behavior, as each relative state can be controlled by the two ends of the relative vector. Moreover, actuation in one only satellite will not only affect to its individual state but will have a global influence on the state of the whole formation through all the relative states that are being perturbed by this only actuation.

Within this situation we could give the satellites the capability to collectively implement formation-wide commands. An optimal combination of thruster commands at each satellite will come to an optimal controller in a global sense.

In fact, this kind of controller architecture can be identified as a whole Multi-Input Multi-Output (MIMO) system, where the inputs are all the thruster commands of the fleet and the outputs are all the relative states that can be defined through it.

We are now in position to implement state-feedback controllers designed with respect to formation-wide objective functions, such as tracking relative vectors between satellites or minimizing the fuel use across the formation.

It is worth mentioning that this represents a centralized solution in the sense that the algorithm takes into account the states of the whole formation but it is decentralized in the sense that there exists no dependency on any specific satellite and each of them computes the control commands by its own means as long as it gets the states of the whole formation.

At this point, one could think that the complexity and the information requirements of the approach taken here may outweigh any advantage that it might prove and that having a simple decentralized independent controller that would track inertial positions for each satellite already provides a known valid solution. However, the author believes that firstly, even if the tracking of inertial independent position is a sufficient condition for the tracking of relative positioning, it is not a necessary condition and sometimes, as in the case of deep space missions, not even possible. And secondly, the author also believes that a coupled dynamics controller provides performance advantages when designed for a cooperative formation of satellites with an interferometric purpose. The following section shows how this is possible.

2.2 Advantages of coupled dynamics architecture

First of all, it is worth mentioning that as part of the MIMO architectures stability and optimality are characteristics that are achieved in a global sense while some controllers can be locally optimal (independent control) but not globally when put together in a multi-agent system.

2.2.1 Scenario definition

Let us think of a scenario where two satellites are flying in the space and these have to be controlled in order to reach a final position from where they will proceed to the imaging of a celestial object (figure 2.2).

The grey star shapes represent the target positions to reach by each of the satellites, the arrows are showing the common direction of the thruster commands and the celestial object to be imaged is supposed to be far away in perpendicular direction to

Figure 2.2: Scenario definition

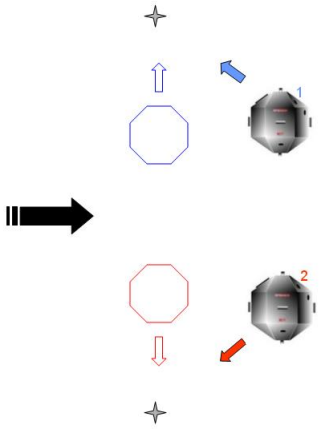

Figure 2.3: Disturbance with independent control

the plan of the figure.

2.2.2 Saving Fuel

Let us suppose now a perturbation –represented with a black arrow– that is pushing both satellites away from their target (figure 2.3).

If satellites are using independent controllers with de-coupled dynamics trying to reach individual inertial positions the common thruster commands will try to fight against this perturbation to eventually reach their target state separately.

However, if those same satellites would be running a controller that uses coupled dynamics and trying to reach the relative state that can be defined subtracting the two target positions, then there would be no need to fight against this perturbation

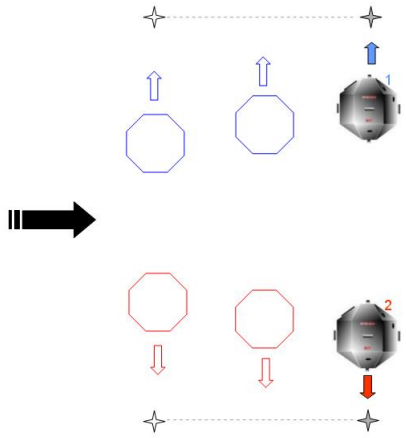

Figure 2.4: Disturbance with coupled dynamics control

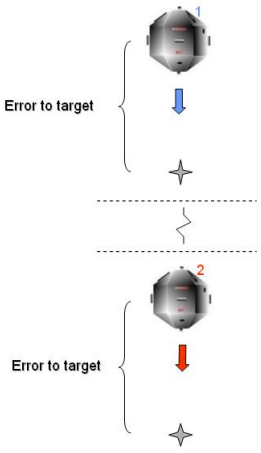

Figure 2.5: Reducing time of response

as the target centroid of the formation is not specified, only the target relative state. In the case where the distance between satellites is low down in orders of magnitude compared to the distance to the celestial object, the target relative vector can freely move in space (free motion of the formation centroid) without affecting the quality of the imaging process at all (figure 2.4).

2.2.3 Reducing Time of Response

Similar conclusions can be reached if we zoom in to a lower scale and consider the error to the target position as the perturbation on the previous case.

Where independent controllers would still try to reach the target positions, the

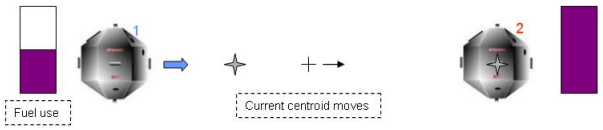

Figure 2.6: Fuel consumption with independent control

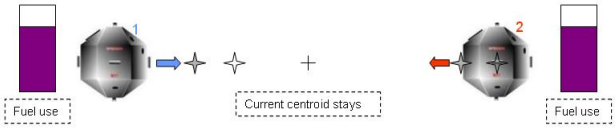

Figure 2.7: Fuel consumption with coupled dynamics control

controller with coupled dynamics will already have reached its final target in the case that both errors to targets are similar. This means that the errors to global positions can be cancelled whenever the situation is given and correction controls will only be commanded in both satellites in order to reach the target relative state which is the real objective of the general scenario definition (figure 2.5).

2.2.4 Balanced fuel use

It is also worth mentioning that due to the fact that all the satellites are connected through the relative states that relate them any maneuver or correction in their states will be executed maintaining an invariant centroid –in a non disturbing environment– which not only leads to the an optimal control for minimizing fuel consumption but it also automatically makes a balanced use of fuel across the formation. In figure 2.6 we can see for the case of an independent controller some maneuvers can lead to a very different use of fuel in between the satellites of the formation.

However, the same maneuver performed with a coupled dynamics controller will have a completely balanced use of fuel by its own, enlarging the lifetime of the mission (figure 2.7).

At the same time, performing the maneuver collectively will again lead to a reduction of the time of response. Instead of having one only satellite executing a long distance maneuver each satellite will perform short distances at the same time giving the reduced time of maneuver.

2.2.5 Performance in tracking error

Let us suppose that an independent de-coupled dynamics controller that is tracking global positions has a tracking error of σ_g. If we would use this controller at each of the two satellites of the described scenario to reach the target global positions the resultant error in relative positioning would be:

$$\begin{aligned} \sigma_{rel}^2 &= \sigma_{g1}^2 + \sigma_{g2}^2 \\ \sigma_{rel} &\approx 1.4\sigma_g \end{aligned} \tag{2.5}$$

However, if the same controller would be adapted to track relative vectors using coupled dynamics we could expect to get a tracking error in relative vectors much lower than $1.4\sigma_g$. Obviously, this relative tracking error cannot be directly predicted from the performance of the independent controller, as we have changed the dynamics of the system and then the controller needs to be re-designed for those. Nevertheless, the open loop poles of the system –eigenvalues of the A matrix in the dynamics equations– have not changed and then we could likely expect to implement a controller that increases the performance in relative positioning reducing the tracking error under $1.4\sigma_g$.

2.2.6 Increased Robustness

The precedent sections provided information about advantageous properties of the coupled dynamics architecture. Many cases showed that the presence of disturbances increases its relevancy and worthiness compared to an independent or decoupled architecture. In fact, the coupled dynamics make the most of the noise that appears to be in the system by reducing the required fuel or the time of response or simply increasing the tracking performance focusing the target states of the formation on relative positioning and not in separated global positions. The robustness against disturbances is increased yet in the insight of this architecture. In the opposite, in an ideal noiseless mathematically perfect situation coupled dynamics would not show any profit in any of these ways. However, there are known external disturbances affecting

the astrodynamics in the out space, solar pressure being surely the most important one. Not only having to consider external sources of orbital perturbations, internal disturbances can also be taken into account in order to prove the general relevancy of using coupled dynamics. Modeling errors in different layers or subsystems, processing noises, estimation error in global position and imperfect identification could be mentioned at this point. In fact, the reasons that make coupled dynamics valuable are the same that boosted the whole theory of close loop control against the mathematically optimal open loop. In other words, the reasons why close loop control is nowadays used for the most part control system would serve to promote the use of coupled dynamics architecture for formation flight control.

2.3 Chapter Summary

This chapter shows the path followed by the author that led to the pre-design of an optimal formation flight control system that uses coupled inter-spacecraft dynamics. Having explained the advantages that this approach may arise for relative positioning between spacecrafts the next chapter will present the scenarios where the architecture has been tested showing also the final design of the controller and the particular implementation for each of the scenarios where it will be tested.

Chapter 3

Optimal Formation Flight Controllers

3.1 Introduction

The previous chapter showed the theoretical advantages of the coupled dynamics architecture and this chapter will show results from testing on real hardware.

Next, the scenarios and other architectures considered for testing are briefly presented. This is followed by a thorough study of the maneuvers; a nominal target trajectory is generated for each of them. At the same time, specific metrics will be introduced for each case scenario which will lead to the definition of cost functions that will directly evaluate the performance of each experiment. Finally, the controller optimizing those cost functions is designed and implemented using the coupled dynamics architecture. Notice that it is not the objective of this research to study new optimal trajectories that minimize some given metrics but instead the design of optimal controllers that would track a given trajectory under the minimization of some criteria. Throughout this thesis, already existing and well documented techniques for solving optimal control problems will be used and their theoretical development will be introduced as they are required.

3.1.1 Test Scenarios

Let us introduce first the scenarios where the architecture is willing to be tested. Three different scenarios are considered, each of them corresponding to different maneuvers in formation flight that will serve to evaluate the rightness of the hypothesis explained in chapter 2. These three maneuvers have been picked in order to not only provide data from trajectories with different dynamical characteristics, which will be useful to discriminate the cases where using a coupled dynamics architecture shows an increased value, but also for their relevancy in a real mission scenario. Given the predominant interferometric purpose of the formation flight space missions designed up to the moment, the maneuvers will at the same time be those studied to be pertinent for the case, which means that the trajectories followed by the satellites will be those to help cover the maximum points of a UV plan due to the known direct relation between the number of UV points covered and the quality of image [1]. Optimal trajectories for interferometric space missions have already been studied by several authors [31] and most of them would agree that spiral trajectories show this quality.

Following these principles, in the first scenario satellites will follow circular trajectories which have dynamical properties close to those of the spirals. Apart from their invariant radius, these trajectories are non-linear in time as the spirals and will provide useful data for the initial evaluation of the properties of this architecture. Secondly, and growing in complexity, spiral maneuvers will be introduced. Finally, in the last scenario, stop and stare maneuvers will be studied where the stopping points will correspond to those of a spiral trajectory. This last maneuver is of particular interest because of its interferometric value and because of its dynamical properties that mix linear and quadratic functions in time.

3.1.2 Comparing Architectures

Besides the coupled dynamics architecture, data from two other architectures in the same scenarios presented above will be taken for comparison. Varying the coupling level in the dynamics of the satellites the first other architecture presents completely

decoupled dynamics. This is commonly named independent control and each satellite separately tracks global positions. The second one has semi-coupled inter-spacecraft dynamics and is commonly know as cyclic architecture. This one differs from the Leader-Follower one in the fact that the connections between satellites are non hierarchical. The specific implementation for this architecture from which data will be extracted is called cyclic pursuit and presents the intrinsic property of natural convergence to moving formations such as circles or ellipses [15].

Results form those three architectures in each of the scenarios will give us enough data to permit us make conclusions about the real improvement in performance when using coupled dynamics.

Prior to the study of each of the maneuvers and the implementation of optimal controllers for each scenario the author has thought convenient to introduce at this point the technique used in this research for solving the optimal control problem. Known as the Calculus of Variations, it can be found in numerous books [19] and it is introduced below to the better understanding of the reader.

3.2 Variational Approach in Optimal Control Problems

In this section the reader will be introduced in the aforementioned technique Calculus of Variations which theoretically can be applied for solving many optimal control problems. Once the general formulation is presented it will be concretized for the problems of interest in this research.

The objective in solving the optimal problem is to obtain an admissible control u that causes the system:

$$\dot{x}(t) = f(x(t), u(t), t) \tag{3.1}$$

to follow an admissible trajectory x that minimizes the performance cost function:

$$J = h(x(t_f), t_f) + \int_{t_0}^{t_f} g(x(t), u(t), t)dt \tag{3.2}$$

where h is the terminal cost that penalizes the final state of the system and g is the integrated cost in the entire control time. In order to ensure that the dynamics equations of the system (Eq. 3.1) are not violated this requires formulating an augmented cost function that includes these constraints into the equation 3.2 to be optimized.

$$J_{aug} = h(x(t_f), t_f) + \int_{t_0}^{t_f} \left\{ g(x(t), u(t), t) + \psi^{\mathrm{T}}(t) \left[f(x(t), u(t), t) - \dot{x}(t) \right] \right\} dt \tag{3.3}$$

where the Langrange multipliers $\psi(t)$ ([5]) are introduced. Most of the consulted literature would at this point define the Hamiltonian function:

$$H(x(t), u(t), \psi(t), t) = g(x(t), u(t), t) + \psi^{\mathrm{T}}(t) \left[f(x(t), u(t), t) \right] \tag{3.4}$$

That permits the redefinition of the augmented cost function. As follows,

$$J_{aug} = h(x(t_f), t_f) + \int_{t_0}^{t_f} \left\{ H(x(t), u(t), \psi(t), t) - \psi^{\mathrm{T}}(t)\dot{x}(t) \right\} dt \tag{3.5}$$

As it has been stated before, the final goal is to find a minimum of this functional. The next step in the procedure is then to define its derivative with respect to all the dependent functions $(x, \dot{x}, \psi, u, t)$. Since the initial state and time are supposed to be known the variations of the augmented cost function with respect to those can be equaled to zero; this assumption can be made without loss of generality. Then we only need to introduce the variations $\delta x, \delta \dot{x}, \delta u, \delta \psi$ and δt_f which gives for an extremal of the cost function:

$$\begin{aligned}\delta J_{aug} = \left[\tfrac{\partial}{\partial x_f} h(x(t_f), t_f)\right]^{\mathrm{T}} \partial x_f + \left[H(x(t), u(t), \psi(t), t) + \tfrac{\partial}{\partial t_f} h(x(t_f), t_f)\right] \partial t_f \\ + \int_{t_0}^{t_f} \{ \left[\tfrac{\partial}{\partial x} H(x(t), u(t), \psi(t), t)\right]^{\mathrm{T}} \partial x \\ + \left[\tfrac{\partial}{\partial u} H(x(t), u(t), \psi(t), t)\right]^{\mathrm{T}} \partial u \\ + \left[\tfrac{\partial}{\partial \psi} H(x(t), u(t), \psi(t), t) - \dot{x}(t)\right]^{\mathrm{T}} \partial \psi + [-\psi(t)]^{\mathrm{T}} \partial \dot{x} \} dt = 0\end{aligned} \tag{3.6}$$

Given the relation between x and $\dot{x}$ we can use the integration by parts technique to rewrite 3.6 into:

$$\begin{aligned}\delta J_{aug} = \left[\tfrac{\partial}{\partial x_f} h(x(t_f), t_f) - \psi(t)\right]^{\mathrm{T}} \partial x_f + \left[H(x(t), u(t), \psi(t), t) + \tfrac{\partial}{\partial t_f} h(x(t_f), t_f)\right] \partial t_f \\ + \int_{t_0}^{t_f} \{ \left[\tfrac{\partial}{\partial x} H(x(t), u(t), \psi(t), t) + \dot{\psi}\right]^{\mathrm{T}} \partial x \\ + \left[\tfrac{\partial}{\partial u} H(x(t), u(t), \psi(t), t)\right]^{\mathrm{T}} \partial u \\ + \left[\tfrac{\partial}{\partial \psi} H(x(t), u(t), \psi(t), t) - \dot{x}(t)\right]^{\mathrm{T}} \partial \psi \} dt = 0\end{aligned} \tag{3.7}$$

Analyzing equation 3.7 we conclude that the integral must vanish on the extremal regardless the boundary conditions. Thus, leading us to the definition of the **necessary conditions**:

$$t \in [t_0, t_f] \begin{cases} \dot{x} = \tfrac{\partial}{\partial \psi} H(x(t), u(t), \psi(t), t) \\ 0 = \tfrac{\partial}{\partial u} H(x(t), u(t), \psi(t), t) \\ \dot{\psi} = -\tfrac{\partial}{\partial x} H(x(t), u(t), \psi(t), t) \end{cases} \tag{3.8}$$

The first equation in 3.8 is known as the state function and it can be easily identified as the dynamics equation of the system given in 3.1 which means that the solution must be one admissible trajectory.

The second one occurs from the fact that the variation in ∂u is independent and must minimize the Hamiltonian. The expansion of this equation leads to the expression of the optimal control command law:

$$0 = \frac{\partial}{\partial u} g(x(t), u(t), t) + \left[\frac{\partial}{\partial u} f(x(t), u(t), t) \right]^{\mathrm{T}} \psi(t) \tag{3.9}$$

Note that this expression is valid under the assumption that the control-efforts are not bounded. In the other case, this equation should be modified to incorporate this additional constraint. Besides, to ensure that the actual $u^*(t)$ causes a local minimum in the Hamiltonian it is sufficient to guarantee that $\frac{\partial^2}{\partial u^2} H(x(t), u(t), \psi(t), t)$ is positive definite[21].

The third equation, known as the co-state equation, is usually the key to solving the optimal control problem. Estimating the co-state will give the actual function of the optimal control command and this can be used for integrating the trajectory. However, solving the co-state equation can be a tedious work depending on the form of the dynamics equations and the cost function. What is more, its complexity grows as the number of states increases.

Note that the missing equations for reaching the optimal solution are given by the **boundary conditions** that are already present in the variation of the augmented cost and that can be divided in three general groups: initial, intermediate and terminal conditions. For the concern of this research only the initial and terminal conditions are discussed. If any further information about boundary conditions were required those are well documented in [19].

Boundary conditions can occur in different expressions depending on the problem statement. As it has already been mentioned, the initial time and state are supposed to be known which for aerospace engineering guaranties that the engineer will have in advance a precise estimate of the position and velocity of the spacecraft. This is a very reasonable assumption.

On the other hand, terminal conditions must be satisfied. Taking the terms outside of the integral in 3.7 and since the variation must be zero, we have:

$$\left[\frac{\partial}{\partial x_f} h(x(t_f), t_f) - \psi(t) \right]^{\mathrm{T}} \partial x_f + \left[H(x(t), u(t), \psi(t), t) + \frac{\partial}{\partial t_f} h(x(t_f), t_f) \right] \partial t_f = 0 \tag{3.10}$$

Supposing that variations on terminal states and terminal time are independent, equation 3.10 can be separated into:

$$\begin{gathered} \frac{\partial}{\partial x_f} h(x(t_f), t_f) - \psi(t_f) = 0 \\ H(x(t_f), u(t_f), \psi(t_f), t_f) + \frac{\partial}{\partial t_f} h(x(t_f), t_f) = 0 \end{gathered} \tag{3.11}$$

where both need to be satisfied separately. The final expression of the terminal conditions will depend on the definition of the problem. If the final state is specified, first equation in 3.11 is ignored while if the final time is specified, then the second one, also known as transversality condition, should be obviated. In this thesis, the final state will be usually specified while the time will be a variable in the optimizing process that will have to be balanced with the fuel consumption.

3.3 Linear Quadratic Regulator

In this section we shall consider an important class of optimal control problems, linear quadratic regulators. The formulation in the previous section states that the dynamics and the cost of the system are function of the states, control and time but does not make any assumption about their form. We shall consider now the case of linear dynamics and quadratic cost. This is a generally valid assumption as complex non-linear dynamics tend to be linearized around a stable point and cost functions can be written as quadratic forms of control efforts and the state. We shall show how in this case the optimal control law can be found as a linear function of the states of the system.

Next, general equations for the LQ formalism in aerospace framework will be introduced in order to find the particular necessary conditions in the formulation of the previous section. The following development is primarily due to R. E. Kalman [16],[17].

Consider the plant described by the linear equations:

$$\dot{x}(t) = A(t)x(t) + B(t)u(t) \tag{3.12}$$

and the quadratic cost function to be minimized:

$$J = \frac{1}{2}x_f^{\mathrm{T}} F x_f + \frac{1}{2}\int_{t_0}^{t_f} \left\{ x^{\mathrm{T}}(t)Q(t)x(t) + u^{\mathrm{T}}(t)R(t)u(t) \right\} dt \tag{3.13}$$

Where H and Q are real symmetric positive semi-definite matrices and R is real symmetric positive definite matrix. The next physical interpretation about the cost function can be made at this point: it is desired to maintain the state vector close to the origin without and excessive expenditure of control effort, where the weighting of Q and R matrices will determine the behavior of the controller to be either expensive-reactive type (Q highly weigthen relative to R) or inexpensive-non-reactive type (R highly weigthen relative to Q). The Hamiltonian is defined:

$$H(x(t), u(t), \psi(t), t) = \frac{1}{2}x^{\mathrm{T}}(t)Q(t)x(t) + \frac{1}{2}u^{\mathrm{T}}(t)R(t)u(t) + \psi^{\mathrm{T}}\left[A(t)x(t) + B(t)u(t)\right] \tag{3.14}$$

And the necessary conditions become:

$$\begin{aligned} \dot{x}(t) &= A(t)x(t) + B(t)u(t) \\ 0 &= \tfrac{\partial}{\partial u}H = R(t)u(t) + B^{\mathrm{T}}(t)\psi(t) \\ \dot{\psi}(t) &= -Q(t)x(t) - A^{\mathrm{T}}(t)\psi(t) \end{aligned} \tag{3.15}$$

The second equation can be solved to get the optimal control law:

$$u^*(t) = -R^{-1}(t)B^{\mathrm{T}}(t)\psi^*(t) \tag{3.16}$$

Choosing R to be positive definite we ensure the existence of R^{-1} and the optimality of the Hamiltonian as $\frac{\partial^2}{\partial u^2}H = R$. Taking the result in 3.16 and substituting into 3.15, the state and co-state equations can be rewritten using matricial nomenclature where these are linear combination of themselves.

$$\begin{bmatrix} \dot{x}^*(t) \\ \dot{\psi}^*(t) \end{bmatrix} = \begin{bmatrix} A(t) & -B(t)R^{-1}(t)B^{\mathrm{T}}(t) \\ -Q(t) & -A^{\mathrm{T}}(t) \end{bmatrix} \begin{bmatrix} x^*(t) \\ \psi^*(t) \end{bmatrix} \tag{3.17}$$

From the theory of control we know that the $2n$ ($n = number\,of\,states$) homogeneous differential equations in 3.17 have the solution of the form (see [19] for further development):

$$\begin{bmatrix} \dot{x}^*(t) \\ \dot{\psi}^*(t) \end{bmatrix} = \varphi(t_f, t) \begin{bmatrix} x^*(t) \\ \psi^*(t) \end{bmatrix} \tag{3.18}$$

and,

$$\dot{\psi}^*(t) = P(t)\dot{x}^*(t) \tag{3.19}$$

However, finding $P(t)$ through the transition matrix $\varphi(t)$ can be a long time consuming task mostly when the order of the system is large and then numerical procedures have to be used. In this research another approach is taken as it can be shown (see appendix) that the matrix P satisfies the matrix differential equation:

$$\dot{P}(t) = -P(t)A(t) - A^{\mathrm{T}}(t)P(t) - Q(t) + P(t)B(t)R^{-1}(t)B^{\mathrm{T}}(t)P(t) \tag{3.20}$$

where the boundary condition is $P(t_f) = F$.

A case of special relevancy is considered when the system is to be controlled for an interval of infinite (non-specified) duration. Kalman has shown that if the next hypotheses are satisfied:

1. System is completely controllable
2. F = 0 (infinite horizon)
3. A, B, R and Q are constant matrices

then $\dot{P}(t) \to 0$ as $tf \to \infty$. Substituting in 3.16:

$$u^*(t) = R^{-1}BPx(t) = -Kx(t) \tag{3.21}$$

we conclude that the optimal control law is a linear combination of the states of

the system. In fact, a constant set of gains (matrix K) can be used to implement a state-feedback controller that stabilizes the system at the origin and minimizes the cost function in 3.13. Matrix P may be found solving the Riccati equation:

$$0 = -PA - A^{\mathrm{T}}P - Q + PBR^{-1}B^{\mathrm{T}}P \tag{3.22}$$

Note that the hypotheses made above for finding the optimal state-feedback time-invariant controller are common assumptions. We can suppose that the matrices defining the linear dynamics of the system stay invariant for the maneuver time and that its duration is not specified a priori and could suffer variations depending on the requirements of each case. Finally, having a controllable system is a valid assumption for the research conducted in here.

3.4 Circular Maneuver

3.4.1 Trajectory Generation

In the first scenario under study satellites will track a circular trajectory. A general expression for this is (figure 3.1):

$$x(t) = r{\cdot}cos(\omega t + \varphi)\hat{e}_1 + r{\cdot}sin(\omega t + \varphi)\hat{e}_2 \tag{3.23}$$

Variations on the radius (r) will cause in larger or smaller circles. Taking into account the dimensions of the air table and the test volume of the ISS the radius was fixed at 0.3m for testing on the table and 0.4m for testing in the ISS. Vectors $\hat{e}_1$ and $\hat{e}_2$ fix the plan on the inertial frame where the circle is placed. φ is the initial phase of the satellite on the circular trajectory. And finally, ω is used to fix the revolution rate of the satellite.

$$\omega = 2\pi/T \equiv revolution\,rate \qquad with\ \ T = revolution\,period \tag{3.24}$$

The revolution period is picked so that the satellites do not exceed the maximum

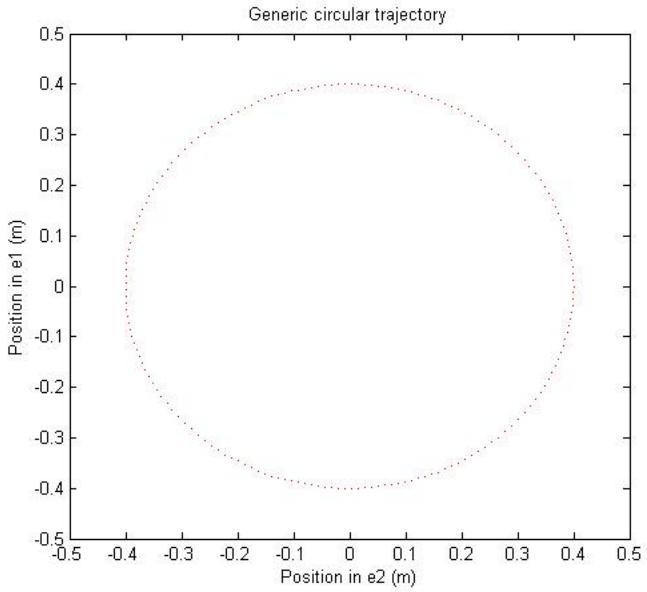

Figure 3.1: Generic circular trajectory

centripetal acceleration they can supply. Given a radius for a circle its perimeter is fixed, changing the period will make the required velocity to vary and this one should not exceed the value that gives the maximum centripetal acceleration. This last one is determined by the thruster capacity of the spheres.

$$\begin{aligned} mV_{max}^2/r &= u_{max} \\ 2\pi r/V_{max} &< T \end{aligned} \tag{3.25}$$

where V_{max} is the maximum magnitude of the velocity vector and u_{max} is the maximun truster force.

which can be rewritten:

$$m{\cdot}r{\cdot}\omega_{max}^2 = u_{max} \tag{3.26}$$

Given the maximum revolution rate the actual rate is picked keeping a security margin so that this nominally required force does not allocate a substantial part of the thrusting capacity.

This maneuver has been run using a formation of two satellites and a revolution period of 180s, which fulfills the requirements just mentioned. The unitary vectors $\hat{e}_1$

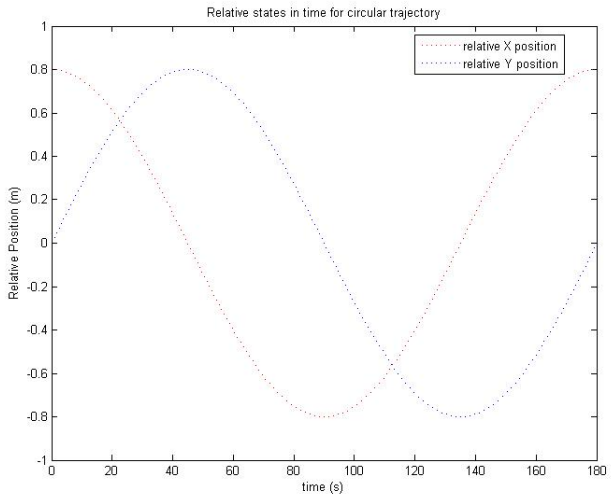

Figure 3.2: Relative states in time for circular trajectory

and $\hat{e}_2$ were chosen to be the $\hat{x}$ and $\hat{y}$ directions of the inertial frame for simplicity. In order to generate the trajectory in relative positioning two global trajectories are subtracted picking the initial phases for each of the satellites to be diametrically opposite, 0 and π.

$$\begin{aligned} p_{rel}(t) &= r{\cdot}cos(\omega t)\hat{x} + r{\cdot}sin(\omega t)\hat{y} - (r{\cdot}cos(\omega t + \pi)\hat{x} + r{\cdot}sin(\omega t + \pi)\hat{y}) \\ &= 2{\cdot}r{\cdot}cos(\omega t)\hat{x} + 2{\cdot}r{\cdot}sin(\omega t)\hat{y} \end{aligned} \tag{3.27}$$

The resulting relative trajectory has exactly the same expression with an increased radius (figures 3.2 and 3.3).

3.4.2 Cost Function

As it has been mentioned before, formation flying space missions are being studied for interferometric purposes because of their excellent performances to observe celestial objects while requiring little orbiting mass. The technological challenge lies on the high precision in relative positioning that interferometer techniques require in order to combine constructively the light coming from each of the collectors, i.e. satellites. It is well understood that, the less the error in relative position the better the quality

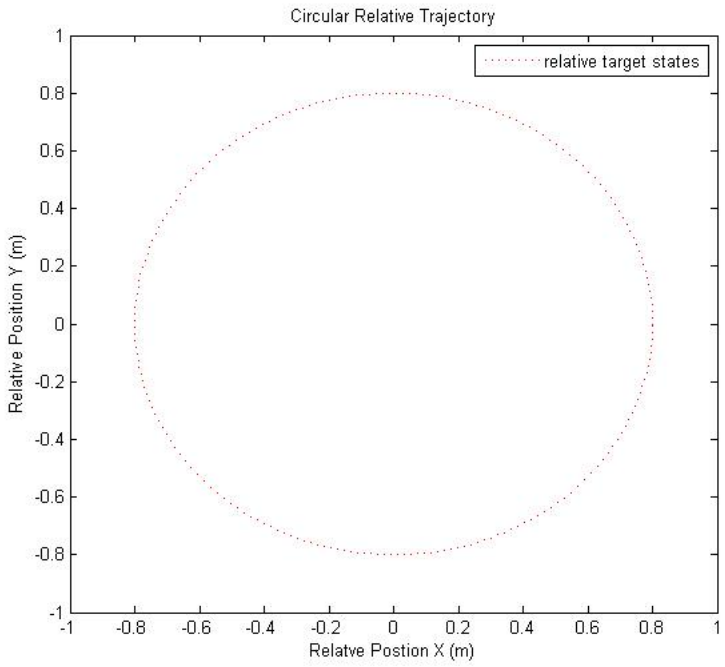

Figure 3.3: Circular relative trajectory

of the image obtained.

It is also worth mentioning that in order to avoid the relatively fast dynamics of an Earth orbiting satellite and so facilitate the control of the formation, this kind of observational missions are designed to be sent either to the deep space or to the popular Earth trailing Lagrange point, which creates a "gravitation free" environment and which justifies the double integrator plant used in this research.

However, one of the key fundamentals of formation flight space systems is to maximize the returns given the minimal resources that are available. The fact of minimizing the use of resources while keeping an acceptable science output becomes then a key aspect on the problem. This will be rewarded with a longer mission lifetime which makes the economical investment worthwhile.

This is why the performance of an experiment cannot only be evaluated for its precision in trajectory tracking but it also needs to take into account the amount of fuel used on this purpose. Considering these metrics a cost function can be defined as a combination of the error in relative position (e) and the energy spent during the

maneuver:

$$J = e^{\mathrm{T}} Q e + u^{\mathrm{T}} R u \tag{3.28}$$

where Q and R are definite positive and usually diagonal matrices. Weighting the values of the matrices will provide a realistic evaluation of the performance.

3.4.3 Controller Implementation

The implementation of the controller will consist on solving the optimal control problem that will minimize the cost function defined in equation 3.28 under the constraints of the coupled inter-spacecraft dynamics of the system. As the coupled dynamics have a linear form and the defined cost function is quadratic the LQ formalism can be applied for solving the optimal control problem. However, note that the LQ controller is supposed to stabilize the state of the system at the origin and we are willing to use it to track a circular trajectory. This is easily overtaken by changing the inputs of the controller and feeding the error to the target state instead of the state of the system itself. This was in fact implicitly assumed in the definition of the cost function. The controller will then try to continuously stabilize the error at the origin, i.e. minimize the tracking error while using an acceptable amount of propellant.

The LQ formalism, as it has been presented before, leads to a state-feedback controller that can be identified as a Proportional Derivative (PD) controller. However, the author has believed that incorporating an integral part to the controller could help minimize the tracking error by rejecting any present disturbances. The way to add the integral contribution to the controller and make it part of the solution of the optimal control problem is by adding an equation to the linearized dynamics. The state vector is incremented where the new state corresponds to the integral of the error (e_{int}). The equation that must be added to the dynamics is:

$$\dot{e}_{int} = p_{reldesired} - p_{rel} = e \tag{3.29}$$

The A, B and C matrices must be augmented, the general reformulation is:

$$A_{aug} = \begin{bmatrix} A_{nxn} \\ -1\,0\,\cdots\,0 \end{bmatrix}$$

$$B_{aug} = \begin{bmatrix} B \\ 0\,\cdots\,0 \end{bmatrix} \tag{3.30}$$

$$C_{aug} = I_{n+1}$$

Let us now use this formulation for implementing the optimal controller using coupled inter-spacecraft dynamics.

In the present, a formation of two satellites is considered. The state vector is defined:

$$x_{for} = [p_{rel}, v_{rel}, e_{int}] \tag{3.31}$$

corresponding to the relative position, velocity, and the integral of the error in relative position. The relative states are defined subtracting the global states of the two satellites.

In this research the convention that the relative state is always defined as the vector going from satellite number one (logical ID1) to satellite number two (logical ID2) has been made.

$$[p_{rel}, v_{rel}] = x_{sat2} - x_{sat1} \tag{3.32}$$

Using the standard linearized dynamics formulation:

$$\dot{x}_{for} = Ax_{for} + Bu \tag{3.33}$$

where,

$$A = \begin{bmatrix} 0 & 1 & 0 \\ 0 & 0 & 0 \\ -1 & 0 & 0 \end{bmatrix}$$
$$B = \frac{1}{m} \begin{bmatrix} 0 & 0 \\ -1 & 1 \\ 0 & 0 \end{bmatrix} \tag{3.34}$$

Note that the control in each of the directions of the axes of the inertial reference frame is done separately as their dynamics are supposed decoupled. Then, the control u is the column vector that takes the thrusting forces of the two satellites in one axis.

Once that the Q and R matrices are chosen (see Bryson's rule section in this chapter) the LQ formalism can be used to compute the PID optimal control law that minimizes the cost function above and that can be formulated by means of the time-invariant matrix K:

$$u = -Kx_{for} \tag{3.35}$$

It is worth mentioning that thanks to the coupled dynamics introduced in the design of the controller this is a globally optimal decentralized controller (see chapter 2).

3.5 Spiral Maneuver

3.5.1 Trajectory Generation

On the second maneuver considered in this research the satellites will follow a spiral trajectory. The spiral was chosen to be of Archimedean type. A general expression for this kind of trajectory is (figure 3.4):

$$x(t) = r(t) \cdot cos(\omega t + \varphi)\hat{e}_1 + r(t) \cdot sin(\omega t + \varphi)\hat{e}_2 \tag{3.36}$$

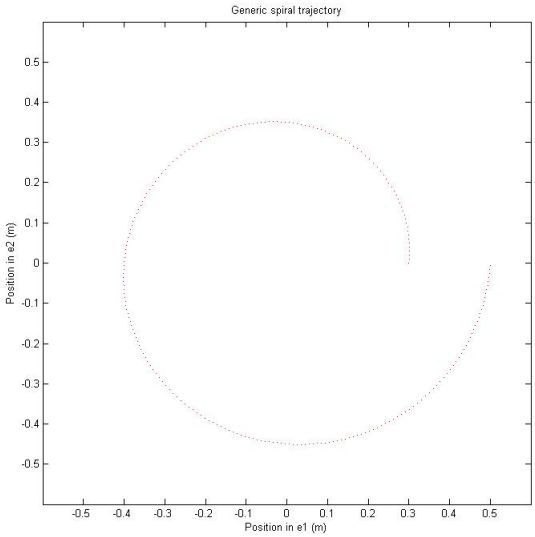

Figure 3.4: Generic spiral trajectory

where $r(t)$ is a linear function of time,

$$r(t) = \alpha \cdot t + r_0 \tag{3.37}$$

where r_0 is the initial radius and α is the rate of the increasing radius.

For the same reason mentioned in the circular maneuver section, α and ω are both picked so that the centripetal acceleration does not exceed the thruster capacity but in this case at any time during the maneuver. α will determine the final radius for a given maneuver time. The radius at the end of the maneuver will be used for selecting ω as the biggest radius is the most restrictive one.

This maneuver has been run using a formation of two satellites, with a radius that goes from 0.2m to 0.4m for air table testing and from 0.3m to 0.5m for testing in the ISS in one only cycle of 180s.

As proceeded for the circular maneuver the relative trajectory is obtained subtracting two global trajectories where the initial phases for each of the satellites are diametrically opposite, 0 and π.

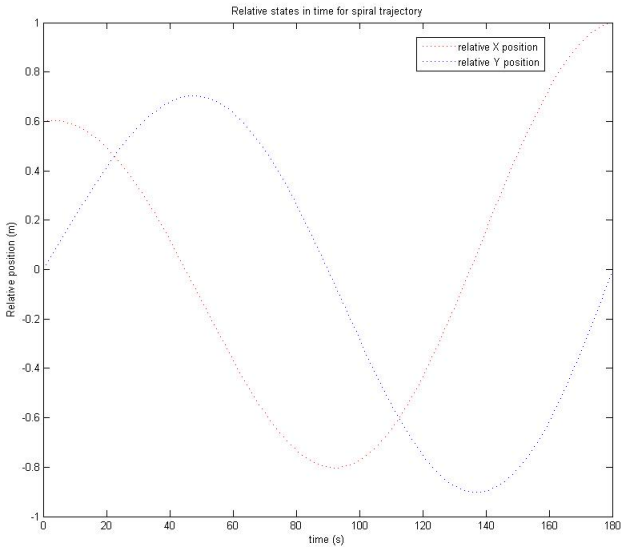

Figure 3.5: Relative states in time for spiral trajectory

$$\begin{aligned} p_{rel}(t) &= r(t)\cdot cos(\omega t)\hat{x} + r(t)\cdot sin(\omega t)\hat{y} - (r(t)\cdot cos(\omega t + \pi)\hat{x} + r(t)\cdot sin(\omega t + \pi)\hat{y}) \\ &= 2\cdot r(t)\cdot cos(\omega t)\hat{x} + 2\cdot r(t)\cdot sin(\omega t)\hat{y} \end{aligned} \tag{3.38}$$

Once again, the resulting relative trajectory has exactly the same expression with doubled radius (figures 3.5 and 3.6).

3.5.2 Cost Function

Considering the similarities between the previous and this maneuver the cost function that would determine the criteria to minimize will also be written as a combination of the tracking error in relative positioning and the energy spent in this purpose:

$$J = e^{\mathrm{T}}Qe + u^{\mathrm{T}}Ru \tag{3.39}$$

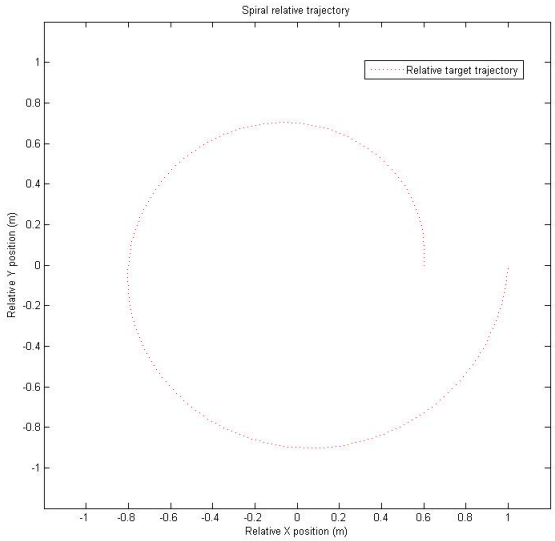

Figure 3.6: Spiral relative trajectory

3.5.3 Controller Implementation

The same coupled inter-spacecraft dynamics and same cost function as used for the circular maneuver lead to the optimal PID controller of the same form:

$$u = -Kx_{for} \tag{3.40}$$

However, the author has believed pertinent adding to the controller for this maneuver a feedforward control that corresponds to the nominal force that would be commanded in an ideal noise-free environment in order to make the satellite follow the target trajectory. This force can be identified as the nominal centripetal force and can be easily calculated at each control period.

$$F = \frac{m \left\| v_{rel} \right\|^2}{\left(\frac{1}{2} p_{rel}\right)} \tag{3.41}$$

Note that for satellite number one the nominal force has the direction of the target relative position while for the satellite number two the direction is the opposite.

3.6 Stop and Stare Maneuver

3.6.1 Trajectory Generation

The third scenario that we will consider in this study is commonly known as Stop and Stare maneuver. This is the popular name is given to interferometric maneuvers where a satellite goes from an initial position to another final position and stops there. This general description is usually corresponded to the maneuver that connects two different image captures or for a formation flight space telescope two different points of the UV plan of the same image. The only specification for this maneuver is the final position and final zero velocity.

Depending on the fuel usage this maneuvers can be performed following different trajectories. However, all these possible trajectories comprise three phases: accelerating, coasting and decelerating phase. The fuel spent in the maneuver will just vary the duration of these phases.

For initial zero velocities the nominal duration of the accelerating and decelerating phases is the same. In the coasting phase the satellite drifts without thrusting. If no restrictions on the use of fuel are made the coasting phase has zero duration and the satellite accelerates up to the half-way and decelerates for the rest of the maneuver. Two generic examples of Stop and Stare maneuver trajectories are shown in figure 3.7, the second one being less fuel demanding.

This trajectory profile is commonly known as Bang-off-Bang type.

Given that the trajectory will depend on the propellant spent and this is one of the optimization variables of the problem we cannot present at this point a nominal target trajectory for this maneuver.

3.6.2 Cost Function

As it has been mentioned before, the only specifications for this maneuver are in fact the terminal conditions: final position and zero velocity. The trajectory followed to reach them can be determined by the optimal controller that would minimize a

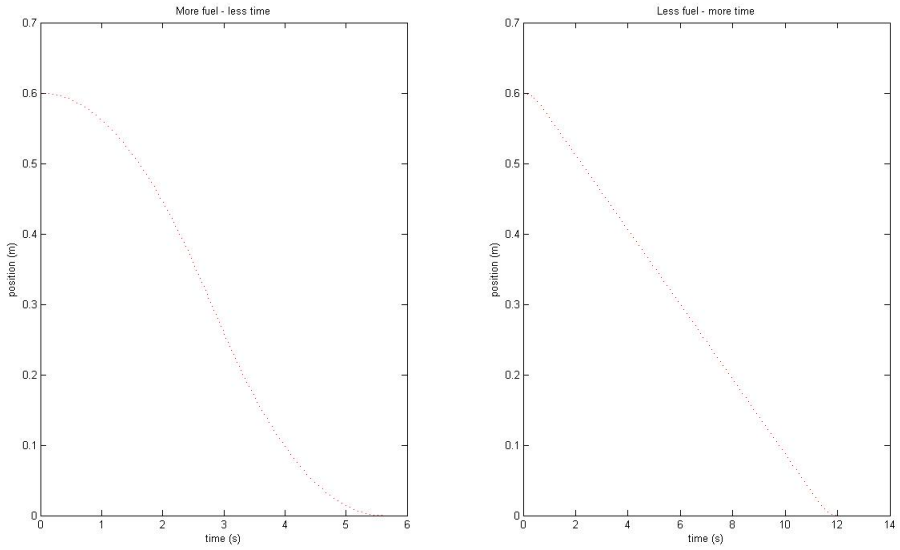

Figure 3.7: Generic Stop and Stare trajectories

specific criterion. However, if we define the cost being only function of the fuel usage the solution to the optimal control problem will return a fuel optimal trajectory with coasting time tending to infinite. This is why the time spent in the maneuver needs to be also penalized. Thus, the cost function for the Stop and Stare maneuver is defined:

$$J = \int_{t_0}^{t_f} 1 + \beta |u(t)| dt \tag{3.42}$$

The variable β serves for the balancing between the time and the fuel used and it will determine the optimal target trajectory to be more or less fuel consuming (see figure 3.7).

3.6.3 Controller Implementation

The reader might predict that the LQ framework is not suitable anymore for the implementation of the optimal controller in the Stop and Stare maneuver. Let us nevertheless explain why this solution could neither intuitively be a good one.

The main reason is not in fact the non quadratic form of te cost function; neither

that the trajectory is not defined in advance, because we could generate a specific Bang-off-Bang trajectory by fixing the amount of fuel used and choose a quadratic cost to follow it as it has been done in the previous maneuvers. The problem arises indeed when noticing that this maneuver combines parts where the trajectory is linear in time (coasting phase) and parts where the trajectory is quadratic in time (accelerating and decelerating). Moreover, minimizing the lag in the accelerating phase and the overshoot in the decelerating phase will be a key factor for the optimality of the controller; those phenomenons would only cause a deficient use of fuel and a longer required time for the maneuver.

A time-invariant state-feedback linear controller like the one given by the LQ formulation and used in previous maneuvers would hardly track such a trajectory without showing a big lag and overshoot, due to the non-anticipatory behavior of the controller. The optimality can only be reached with a Bang-off-Bang firing profile which comprises two open firing phases connected by a drifting (non-firing) phase. And this again is not the profile that would show a time-invariant LQ controller.

Herein, we intend now to solve the optimal control problem by means of the Calculus of Variations that will minimize the cost function above and will reach some given terminal conditions within an admissible trajectory constrained by the couple dynamics of the system. Consider the double integrator plant with the relative position and velocity as state vector and the thrusting forces of two satellites as control commands:

$$\begin{gathered}
\dot{x}_{for} = [p_{rel}, \dot{v}_{rel}] = Ax_{for} + Bu \\
A = \begin{bmatrix} 0 & 1 \\ 0 & 0 \end{bmatrix} \\
B = \tfrac{1}{m} \begin{bmatrix} 0 & 0 \\ -1 & 1 \end{bmatrix} \\
|u_i| < u_{max}
\end{gathered} \tag{3.43}$$

Let us select for this example some random initial relative position p_{rel0} and as terminal condition we will fix the final state at the origin $p_{relf} = 0$.

For the given cost function, the Hamiltonian is defined as:

$$H = 1 + \beta|u| + \begin{bmatrix} \psi_1 & \psi_2 \end{bmatrix} \left\{ \begin{bmatrix} 0 & 1 \\ 0 & 0 \end{bmatrix} \begin{bmatrix} p_{rel} \\ v_{rel} \end{bmatrix} + \frac{1}{m} \begin{bmatrix} 0 & 0 \\ -1 & 1 \end{bmatrix} \begin{bmatrix} u_1 \\ u_2 \end{bmatrix} \right\} \tag{3.44}$$

$$= 1 + \beta|u| + \psi_1 v_{rel} + \psi_2 \frac{1}{m} (-u_1 + u_2)$$

From the necessary conditions that must be satisfied the co-state equation gives:

$$\begin{aligned} \dot{\psi} &= -\tfrac{\partial}{\partial x} H \\ \dot{\psi}_1 &= 0;\ \psi_1 = c_1 \\ \dot{\psi}_2 &= -\psi_1;\ \psi_2 = -c_1 t + c_2 \end{aligned} \tag{3.45}$$

where c_1 and c_2 are constant values to be determined.

The third necessary condition tells us that the optimal control must minimize the Hamiltonian.

$$\frac{\partial}{\partial u} H = 0$$

Analyzing only the parts of the Hamiltonian that depend on the control u:

$$\beta|u_1| + \beta|u_2| + \psi_2 \frac{1}{m} (-u_1 + u_2) \tag{3.46}$$

we conclude that since $\beta > 0$, u_1 and u_2 must have opposite signs so that:

$$(-u_1 + u_2) = \pm (|u_1| + |u_2|) \tag{3.47}$$

We rewrite 3.46 defining $u = \pm(|u1| + |u2|)$:

$$\beta|u| + \psi_2 \frac{1}{m} u \tag{3.48}$$

Note that the Hamiltonian is the sum of two functions $|u|$ and u, sign of which depends on sign and relative size of ψ_2 compared to β.

Three cases need to be considered now:

- If $\psi_2 > \beta > 0 \rightarrow u^* = -2u_{max} \rightarrow u_1^* = u_{max}$, $u_2^* = -u_{max}$
- If $\psi_2 < -\beta \rightarrow u^* = 2u_{max} \rightarrow u_1^* = -u_{max}$, $u_2^* = u_{max}$
- If $\beta > \psi_2 > -\beta \rightarrow u^* = 0 \rightarrow u_1^* = 0$, $u_2^* = 0$

Thus, the optimal control law has the form:

$$u(t) \begin{cases} -2u_{max} & \psi_2 > \beta \\ 0 & \beta > \psi_2 > -\beta \\ 2u_{max} & \psi_2 < -\beta \end{cases} \tag{3.49}$$

we identify this profile as a bang-off-bang type which we already knew was the optimal controller's profile. We can also foresee that, for the given scenario where initial zero velocity is supposed, and since ψ_2 is a linear function of time that only two switches will occur in the control command during the maneuver. Those switches correspond indeed to the ones between the accelerating and the coasting phase and between the coasting and decelerating phase. The effective values of ψ_2 will depend on the boundary conditions i.e. the initial and final states.

Applying the boundary conditions, the transversality condition tells:

$$1 + \beta|u(t_f)| + \psi_2(t_f)\frac{1}{m}u(t_f) = 0 \tag{3.50}$$

Since the system must stop at $t_f \rightarrow u(tf) = \pm 2u_{max}$

$$\begin{aligned} If\, u(t_f) = 2u_{max} \rightarrow \psi_2(t_f) = -\left(\beta + \tfrac{m}{2u_{max}}\right) < \beta \\ If\, u(t_f) = -2u_{max} \rightarrow \psi_2(t_f) = \left(\beta + \tfrac{m}{2u_{max}}\right) > \beta \end{aligned} \tag{3.51}$$

Therefore, the boundary conditions are consistent with the optimal control law in 3.49. So, the initial and terminal states will serve to determine the initial and final signs of the control commands.

The only task left is to determine the switching times and final time for the maneuver. Let us pick an arbitrary initial state $p_{rel0} > 0$. Then, the initial control command should be $u^*(0) = -2u_{max}$ and $\psi_2(0) > \beta$. The first switching point will occur at $t = t_1$ and the second one at $t = t_2$. Then the following equations must be satisfied at the switching points:

$$\begin{aligned} \psi_2(t_1) &= c_2 - c_1 t_1 = \beta \\ \psi_2(t_2 = t_f - t_1) &= c_2 - c_1 (t_f - t_1) = -\beta \end{aligned} \tag{3.52}$$

And since $\psi_2(t_f) = -(\beta + m/(2u_{max})) = c_2 - c_1 t_f$ we get that:

$$\begin{aligned} t_1 &= \tfrac{m}{2u_{max} c_1} \\ t_f &= 2t_1 + \tfrac{2\beta}{c_1} \end{aligned} \tag{3.53}$$

In order to determine c_1 we just need to integrate the trajectory using the switching and finishing times above and solve the Two Point Boundary Problem (TPBP) for the given initial and final states (see Appendix). The solution leads to:

$$c_1^2 = \frac{\left(2\beta + \frac{m}{2u_{max}}\right)}{p_{rel0}} \tag{3.54}$$

Note that if the initial state had been chosen to be $p_{rel0} < 0$, then the trajectory would be symmetric with reference to the origin but the switching and finishing times would remain the same. Thus, the optimal Bang-off-Bang controller could be generally defined for arbitrary initial and terminal states as:

$$u(t) \begin{cases} \pm 2u_{max} & 0 < t < t_1 \\ 0 & t_1 < t < t_f - t_1 \\ \mp 2u_{max} & t_f - t_1 < t < t_f \end{cases} \tag{3.55}$$

where,

$$\begin{aligned} t_1 &= \tfrac{(|p_{rel0} - p_{relf}|)^{\frac{1}{2}} m}{(2u_{max} \cdot (2\beta + m/(2u_{max}))^{\frac{1}{2}})} \\ t_f &= \tfrac{2t_1 + 2\beta(|p_{rel0} - p_{relf}|)^{\frac{1}{2}}}{(2\beta + m/(2u_{max}))^{\frac{1}{2}}} \end{aligned} \tag{3.56}$$

Integrating the control commands within the coupled dynamics we get the optimal relative trajectory ($p_{rel0} > p_{relf} = 0$):

$$p_{rel}(t) \begin{cases} p_{rel0} - \frac{2u_{max}}{m}\frac{1}{2}t^2 & 0 < t < t_1 \\ p_{rel0} - \frac{2u_{max}}{m}\frac{1}{2}t_1^2 - \frac{1}{c_1}(t - t_1) & t_1 < t < t_f - t_1 \\ p_{relf} + \frac{2u_{max}}{m}\frac{1}{2}(t_f - t)^2 & t_f - t_1 < t < t_f \end{cases} \tag{3.57}$$

$$v_{rel}(t) \begin{cases} \frac{2u_{max}}{m}t & 0 < t < t_1 \\ -\frac{1}{c_1} & t_1 < t < t_f - t_1 \\ -\frac{2u_{max}}{m}(t_f - t) & t_f - t_1 < t < t_f \end{cases} \tag{3.58}$$

3.6.3.1 Open loop controller

The solution of the optimal control problem for the stop and stare maneuver is in fact a controller that is pre-defined by the thrusting profile and times in 3.56. Once that beta is picked then the nominal trajectory that optimally brings the system from the initial state to the final one is specified in 3.57. Thus, in a noise-free ideally modeled environment, commanding to the system the controls defined in 3.56 will perfectly track the trajectory in 3.57. However, this is nothing but an optimal open loop control whose main drawback is the non-robustness. The actual noise and disturbances present in the system and the non-perfect identification and modeling of its subsystems make an open loop control hardly worthy. In the next section we will explain how the problem of the low robustness is solved while keeping the optimality of the controller.

3.6.3.2 Phase-Plane controller

Herein, we intend to close the loop so we can make our control commands depend on the actual state of the system instead of following a predefined thrusting profile.

In order to do so let us introduce first what a phase plane graph is. A phase plane graph is a graphical representation that shows the evolution of the states of the

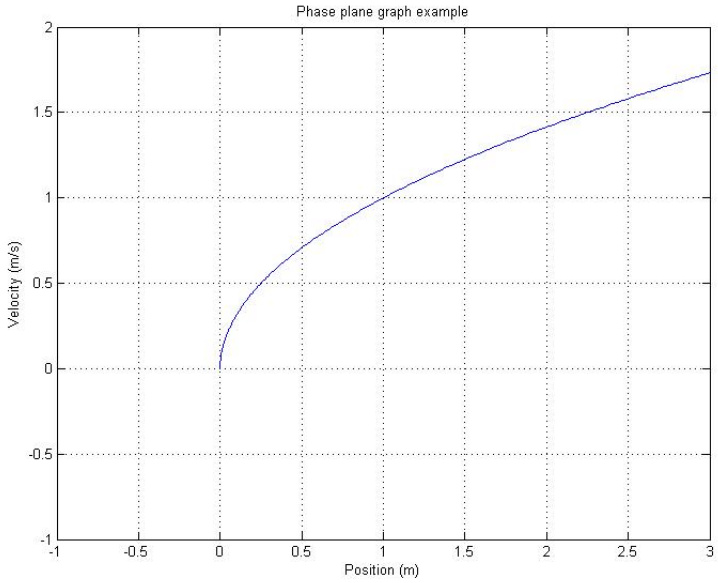

Figure 3.8: Example of phase plane graph

system. Let us chose for example the position and velocity states of a system whose dynamics are defined by a double integrator plant. In that case, we can generate a 2D graph where the states of the system are the axis. Then, a translational motion with positive constant acceleration starting at the origin of coordinates could be represented by the phase plane graph in figure 3.8.

The TPBP mentioned when solving the optimal control problem gives in fact, apart from the switching times, the curves in the phase plane where the switchings occur. While integrating the TPBP (see Appendix) we find that the switchings are placed over the curves:

$$\begin{aligned} p_{rel}(t) &= \left(2\beta + \frac{m}{4u_{max}}\right) v_{rel}^2(t) \Rightarrow first\, switch \\ p_{rel}(t) &= \left(\frac{m}{4u_{max}}\right) v_{rel}^2(t) \Rightarrow second\, switch \end{aligned} \tag{3.59}$$

Figure 3.9 represents those curves in a phase-plane graph for arbitrarily selected β and u_{max}:

Let us suppose an initial positive relative position ($p_{rel0} > 0$) that is asked to be driven to the origin. Then we could represent the trajectory followed by the system over the previous phase plane graph (figure 3.10).

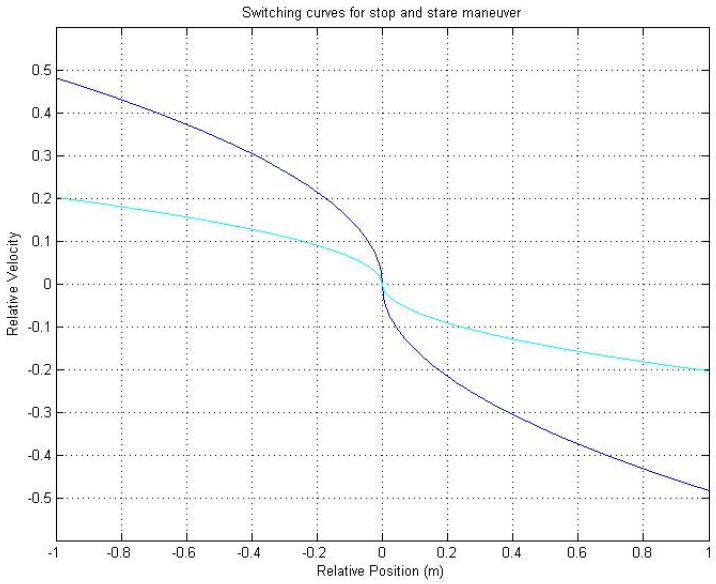

Figure 3.9: Switching curves for Stop and Stare maneuver

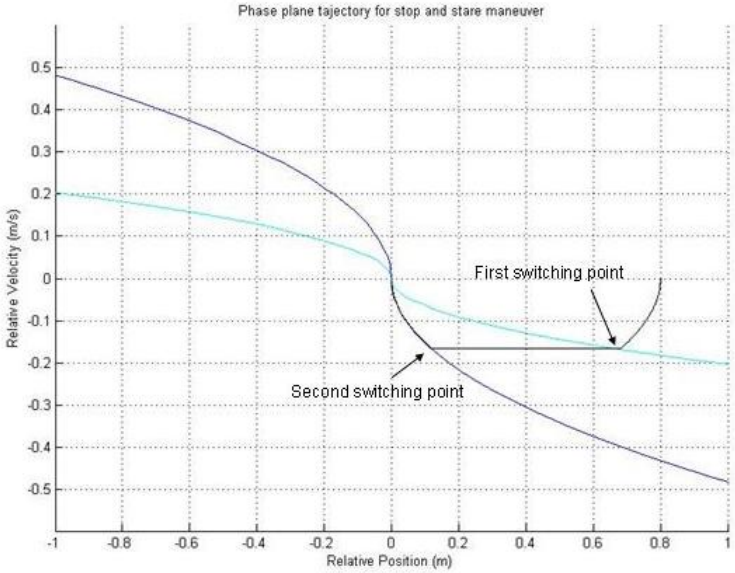

Figure 3.10: Phase-Plane trajectory for Stop and Stare maneuver

In figure 3.10 the three phases of the trajectory (black line) can be identified. In the accelerating phase, the system moves from its initial position towards the origin increasing its velocity (negative acceleration). When the trajectory overtakes the first switching curve (cyan line) the system stops firing leading to the coasting phase with constant velocity. When the second switching curve is reached (blue line), the system starts decelerating until it gets to origin with zero velocity.

Variations on beta will produce changes in the firsts switching curve. For greater values of beta the line becomes more flat and the system has a fuel saving behavior. Lower values of beta will make the first curve get closer to the second one where, in the limit ($\beta = 0$), both are confounded and the system never stops firing as the coasting phase has zero duration.

As it can be noticed, this controller has the same Bag-off-Bang behavior of the open loop controller that was initially found as solution to the optimal control problem. However, instead of following a predefined firing schedule this controller decides whether it needs to accelerate, drift or decelerate depending on the actual state of the system and the switching curves. Thus, the problem of the low robustness of the open loop controller is solved.

This Phase-Plane non linear controller can be said to be the optimal close loop controller for a stop and stare maneuver that minimizes the cost function defined in the previous section.

The Stop and Stare maneuver will be performed by means of the Phase-Plane controller. However, it is worth mentioning that prior to the maneuver and after this precise one satellites need to be stable in fixed relative target positions (image captures). Hence, using the Phase-Plane controller for the static phases of the maneuver is not the best solution. Thus, the LQ controller implemented for the Circular and Spiral maneuvers will be used for the stable phases before and after the Stop and Stare maneuver. In figure 3.11 we can see the timeline of the controllers that are used during different phases of the entire test.

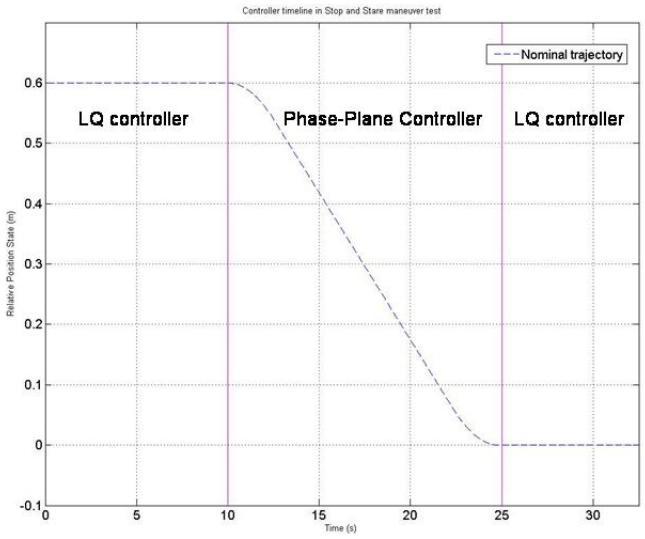

Figure 3.11: Controller timeline in Stop and Stare maneuver test

3.7 Testing on the air table

On the following section results from testing the controllers on SPHERES air table are shown. The three scenarios are tested and the performance improvement by using the coupled inter-spacecraft dynamics is discussed. However, prior to the results analysis some inconvenient situations when testing the coupled dynamics architecture in the SPHERES testbed are treated here below.

3.7.1 Control of the Centroid

Some of the advantages of the coupled dynamics architecture are based on the free-drifting of the formation centroid which leads to a reduction of required fuel. This at the same time makes the satellites concentrate their efforts in tracking the target relative states without caring about their states in a global reference frame.

The SPHERES testbed disposes of two testing environments which are the air table at the Space Systems Laboratory and the ISS laboratory volume. As it can be expected, both of them have limited dimensions. Little imperfections on the table (hard to have a big surface perfectly perpendicular to the gravitational field) will make satellites drift considerably when they are not commanded to hold their position. But,

even in the ISS environment where the satellites do not show a big uncontrolled drift having a free-drifting centroid of the formation is not a secure option and presents the mayor issue that the satellites could end up hitting any wall of the ISS and so invalidate the test before getting useful data. On the air table, a free drifting satellite would hit the edges of the table in less than one minute. For this reason, control of the centroid is required in order to complete the test without exceeding the measures of the test area or volume.

It is worth mentioning that if only the air table would comprise a bigger area, those imperfections would in fact be convenient as they could be modeled as external disturbances and they would probably help proving the reduced fuel usage property of the coupled dynamics architecture.

However, adding a centroid control has a decoupling effect in the dynamics of the system. At some point, where the centroid and relative control efforts were comparables, the satellites dynamics would in fact become decoupled. In order to avoid that situation, we must keep the relative control efforts over the ones of the centroid with a certain margin. This can be made by weighting the feedback gains for the relative and centroid control so that the first ones become more reactive but always keeping the centroid control effective enough so that satellites do not exceed the test limits. The explanation of how the weighting of the gains has been done is given further in this section. Yet, having bigger gains shows another inconvenient effect.

The thruster commands that the controller can apply are bounded. This is a common situation in most of the satellite systems. The impulsion they can thrust is limited and thus so is the maximum applicable force or acceleration. This means that the actuators of the system have in fact a non linear behavior. This kind of non linearity where commands saturate at a certain level has a known undesirable effect. The theory of non linear control has been developed for years and the actuator saturation is probably the most studied non linearity by several authors [18]. When using the state feedback LQ controller, the control commands of the controller (output signal) can be modeled a priori as a linear function of the measured states (input

signal). So, taking the case of the LQ controller:

$$u(t) = -Kx_{for}(t) \tag{3.60}$$

where $u(t)$ is the output signal, $x_{for}(t)$ is the input signal and K is the constant feedback gains matrix. As long as $|u(t)| < u_{max}$, the controller remains inside the linear region and the system's dynamics are fixed by the close loop control. However, when the input signal exceeds a certain limit the command does not satisfy 3.60 anymore. This is instead saturated at a certain value. This behavior can be modeled making the K matrix be function of $x_{for}(t)$.

$$u(t) = -K(x_{for}(t))x_{for}(t) \tag{3.61}$$

Then, the matrix K stays invariant up to a certain input level and then decreases inversely proportional to this one. Whenever the controller exceeds the linear region the close loop control system becomes less and less effective as the control gains are reduced. Analyzing this by means of a root-locus representation we could see how the close loop poles move towards the open loop poles of the system. Eventually, the dynamics of the system are not fixed by the close loop control anymore and the system destabilizes.

3.7.1.1 Increasing the linear margins of the actuator

The SPHERES satellites have a software variable that fixes the amount of time that can be used for thruster firing at each control loop. This variable is called duty_cycle and specifies the percentage of the control period that is allocated for firing. Increasing the duty cycle we enlarge the firing time window at each control loop and thus the maximum applicable force is also increased. This is translated by a larger linear margin in the actuator where the system stays inside the stable region (figure 3.12).

Once the non linearity issue has been solved we just need to make sure that the commanded controls to the actuator never exceed the maximum applicable force so that the actuators always works in between its linear margins and the system

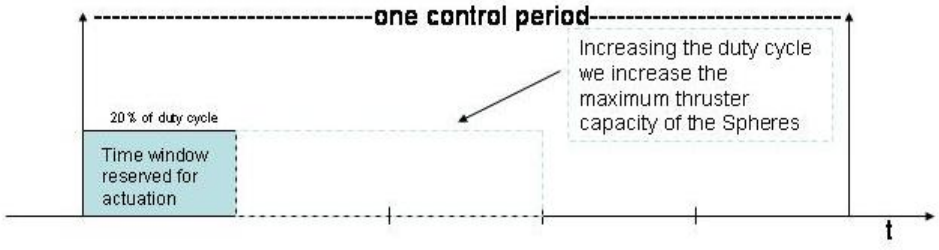

Figure 3.12: Use of duty cycle to increase the maximum thruster capacity of Spheres

does not destabilize. This can be introduced as another constraint equation in the optimal control problem or can also be dealt a posteriori by weighting the gains of the feedback controller. The second approach was taken in this research and its procedure is explained here below.

3.7.1.2 Bryson's rule

In order to solve the Ricatti equation in 3.22, matrix Q and R need to be chosen. The close loop system dynamics will depend on the selected values for those matrices. One of the most followed rules for picking up the values of Q and R is known as Bryson's rule:

$$Q = \begin{bmatrix} \frac{\alpha_1^2}{(x_1)_{max}^2} & & & \\ & \frac{\alpha_2^2}{(x_2)_{max}^2} & & \\ & & \ddots & \\ & & & \frac{\alpha_n^2}{(x_n)_{max}^2} \end{bmatrix}$$

$$R = \rho \begin{bmatrix} \frac{\beta_1^2}{(u_1)_{max}^2} & & & \\ & \frac{\beta_2^2}{(u_2)_{max}^2} & & \\ & & \ddots & \\ & & & \frac{\beta_m^2}{(u_m)_{max}^2} \end{bmatrix} \tag{3.62}$$

- The $(x_i)_{max}$ and $(u_i)_{max}$ represent the largest desired response/control input for that component of the state/actuator signal.
- The $\sum_i \alpha_i^2 = 1$ and $\sum_i \beta_i^2 = 1$ are used to add an additional relative weighting

on the various components of the state/control. These parameters are used in this research to balance the control efforts in relative control and centroid control so that the relative one presents a more reactive response and the dynamics of the satellites remain coupled.

- ρ is used as the last relative weighting between the control and state penalties and gives us a concrete way to discuss the relative size of Q and R. Low values of ρ will produce an underestimated use of fuel with a very reactive system and fast dynamics. On the other hand, fast dynamics means big feedback gains and this will make the actuators reach faster the saturating point. Big values of ρ increase the weight of fuel use in the cost function and the controller becomes less reactive with lower feedback gains. Finally, the value of ρ needs to be chosen so that dynamics are fast enough to present an admissible time of response but keeping the system safe from saturating.

However, the engineer must know that these are just some guidelines for initializing the matrices and reaching the final desirable behavior usually requires of iterative processes where the specific values are tuned.

3.7.2 Results Analysis

In this section results from testing on the air table the implementations of the optimal controllers in each of the scenarios will be shown.

3.7.2.1 Circular Maneuver

Figures 3.13, 3.14 and 3.15 resulted while performing a circular maneuver in SPHERES. This data already served to prove the good behavior of the controller and validate the coupled dynamics architecture as an interesting approach for tracking relative states between satellites. While figure 3.13 shows the satellites' global trajectory on the horizontal table plane -where the circles are noticeable but not very precise- figures 3.14 and 3.15 show the very precise tracking of the relative states during the whole

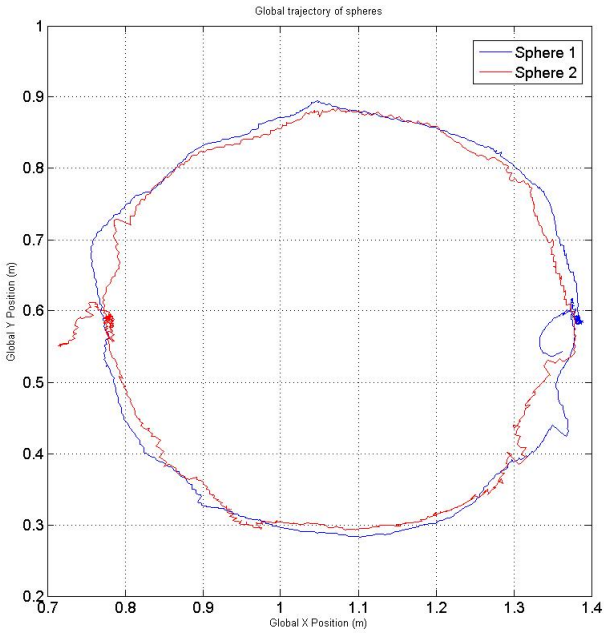

Figure 3.13: Global trajectory of Spheres in circular maneuver, air table test

circular maneuver. Computing the magnitude of the error on the formation plane during the maneuver as:

$$error\,magnitude = \left(error^2_{relXpos} + error^2_{relYpos}\right)^{\frac{1}{2}} \tag{3.63}$$

The mean value of the magnitude for the entire cycle is 1,0cm which is likely the lowest tracking error ever achieved in a circular maneuver on the SPHERES air table.

3.7.2.2 Spiral Maneuver

Next, the spiral maneuver was tested on the SPHERES air table. Once again, while figure 3.16 shows not very accurate spiral global trajectories of the satellites, figures 3.17 and 3.18 demonstrate high precision in the tracking of relative states. The mean value of the error magnitude for the spiral cycle is 1,2cm which is also the state of the art of the SPHERES air table.

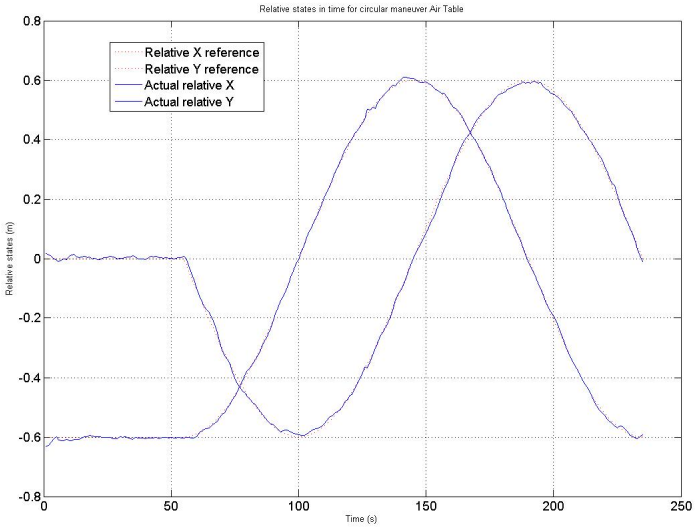

Figure 3.14: Relative position states in time for circular maneuver, air table test

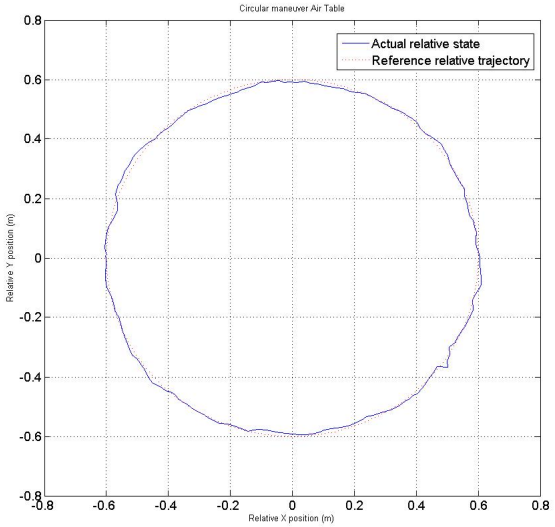

Figure 3.15: Circular maneuver, air table test

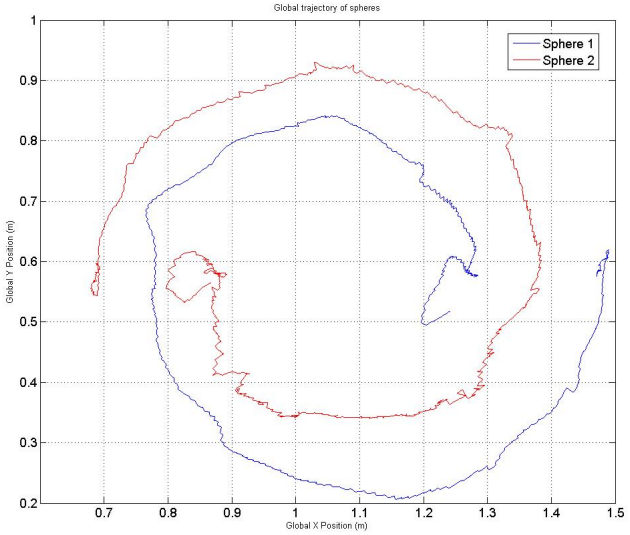

Figure 3.16: Global trajectory of Spheres in spiral maneuver, air table test

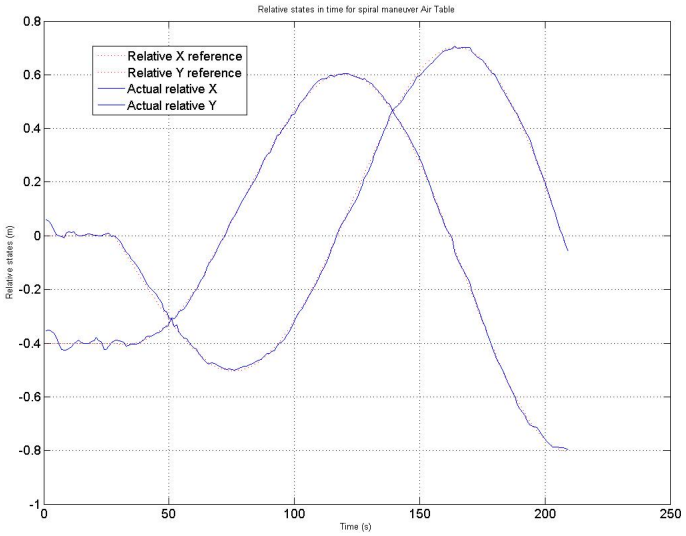

Figure 3.17: Relative position states in time for spiral maneuver, air table test

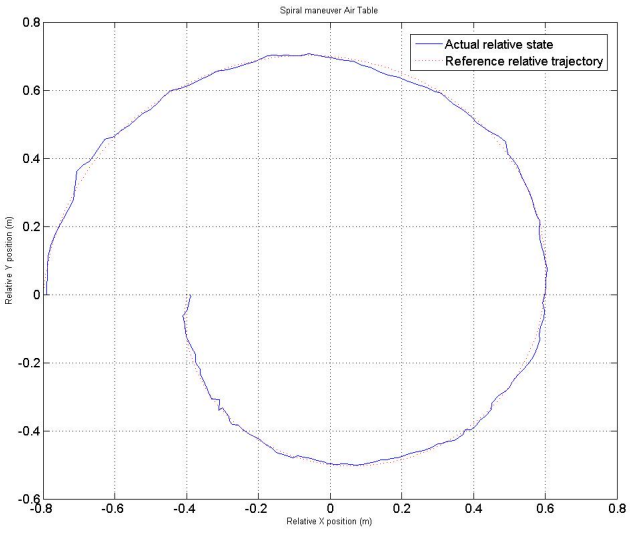

Figure 3.18: Spiral maneuver, air table test

3.7.2.3 Stop and Stare Maneuver

The last tested scenario on the SPHERES air table with the coupled dynamics architecture control was the Stop and Stare maneuver. The optimal controller implemented for this type of trajectory was a close-loop state-feedback non-linear control law named as Phase-Plane controller.

As it has been shown in the section 3.6.3.2 the controller computes the curves on the phase-plane graph where the switchings of the Bang-off-Bang firing profile occur. The controller however, relies on a precise identification of the maximum thrusting force of the satellites (u_{max}), as this is a variable that is used to calculate the curves. Even if we dispose of a precisely identified nominal thrusting force of the satellites, the disturbing environment that is found in the SPHERES air table makes the transmitted acceleration impulse to be time-and-space variant.

Another handicap to be overcome when testing the Phase-Plane controller on SPHERES is the discrete time condition of the control system. Due to this fact the switchings do not occur just over the curves on the phase-plane graph but they occur instead at the very next control step after these lines are crossed over. Depending on the dynamics of the system –how fast these are–, the delay on the switching will

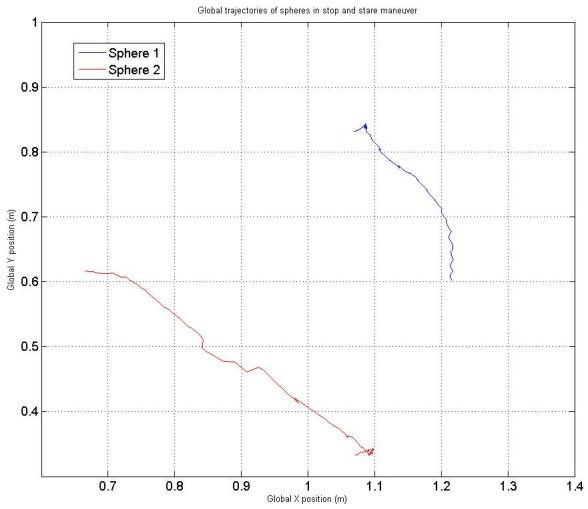

Figure 3.19: Global trajectory of Spheres in Stop and Stare maneuver, air table test

be more or less significant and so they will the lag and overshoot on the tracking of relative states.

Despite these two inconvenient conditions the data obtained when testing the Stop and Stare maneuver on the SPHERES air table was also very satisfactory. The asymmetric different global trajectories followed by the two satellites in figure 3.19 shows the effectiveness of the coupled dynamics architecture. The controller makes the most of the external and internal disturbances present in the SPHERES testing environment deciding to switch to the coasting phase of the maneuver when the necessary relative velocity is acquired even if the satellites have very different global velocities. A reduced use of fuel is guaranteed by this fact.

Figure 3.20 shows the evolution of the relative states in time and figure 3.21 shows the relative trajectory followed by the satellites on the phase-plane graph. The considerably little overshoot assures the efficient use of time and fuel in the maneuver which will be the performance metrics when testing the controller in zero-gravity environment.

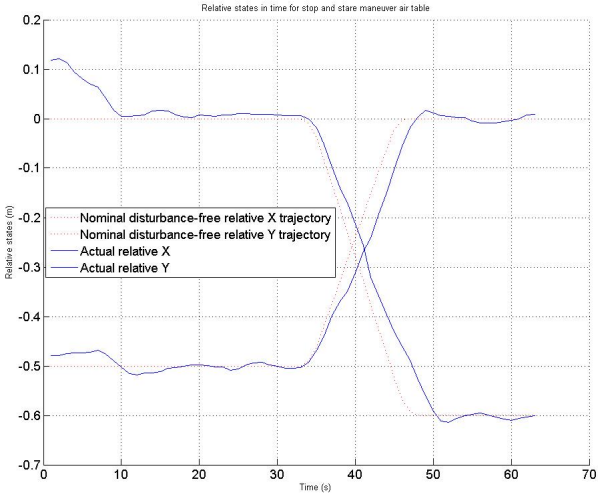

Figure 3.20: Relative position states in time for Stop and Stare maneuver, air table test

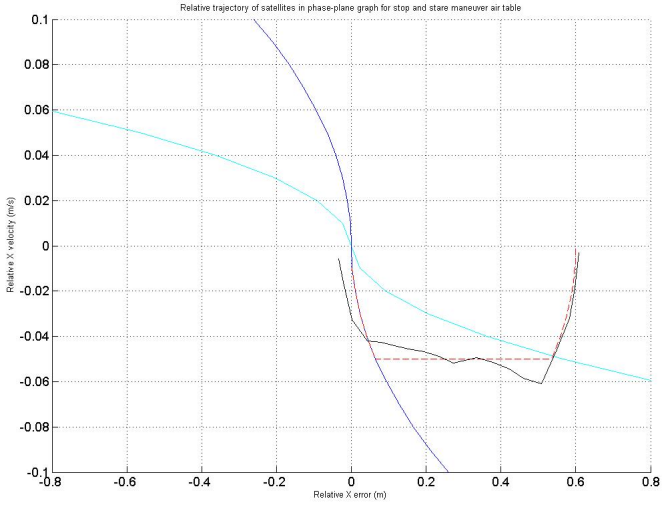

Figure 3.21: Relative trajectory of Spheres in phase-plane graph for Stop and Stare mnaeuver, air table test

3.7.3 Summary of testing on the air table

Testing the coupled dynamics architecture on the SPHERES air table returned very valuable data proving the high accuracy of the controllers when tracking relative trajectories such as circles and spirals and very effective time-fuel consumption when performing a Stop and Stare maneuver.

No further analysis on the fuel usage was made at this point because of the centroid control that had to be added to perform the tests –for the reasons explained in the section 3.7.1 of this chapter– resulting on unnecessarily increased fuel consumption. Thus, analyzing the fuel use on these tests would not be representative or concluding for the evaluation of the coupled dynamics architecture.

At this point the algorithms are considered to be ready to be sent to the NASA headquarters that will be in charge of transferring the test files to the ISS.

3.8 Testing on the ISS

A total of two tests using the coupled dynamics architecture were run during the 19th SPHERES test session in the ISS held on the 26th of August 2009. Those tests corresponded to the circular and spiral maneuvers tested on the SPHERES air table. The following section will analyze the data obtained in those tests and will be compared to data obtained from other tests where circular and spiral maneuvers were performed using other control architectures.

The Stop and Stare maneuver test using the coupled dynamics architecture is scheduled to happen in October 2009 during the 20th SPHERES test session in space. The analysis of this data will be provided in the SPHERES Test Session Report document that is published by the SPHERES team after each test session.

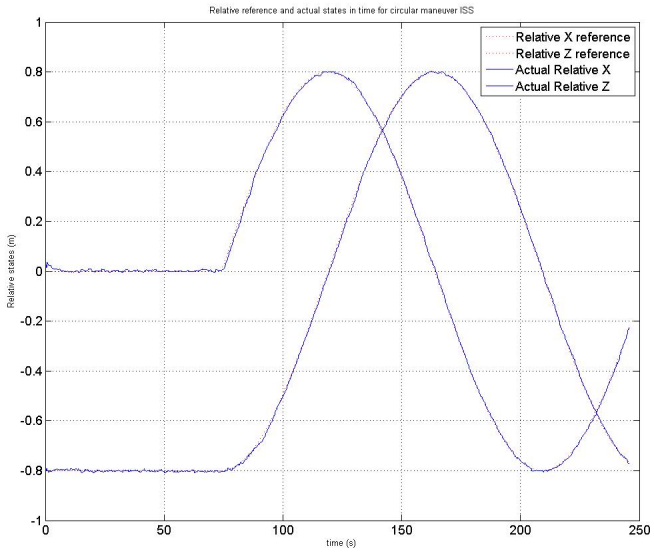

Figure 3.22: Relative position states in time for circular maneuver with coupled dynamics, ISS test

3.8.1 Results Analysis

3.8.1.1 Circular Maneuver

The test performing the circular maneuver was very successful. The gravitational-free low-disturbing environment permitted showing the high precision of the coupled dynamics controller tracking relative states. Figures 3.22 and 3.23 show the evolution of the relative states in time and the relative trajectory on the formation plan followed by the satellites during the circular maneuver. It can be noticed from figure 3.23 that the entire circular cycle was not completed by the satellites. This was due to a low battery level in one of the satellites that caused it to reset. However, the SPHERES Team decided at that moment of the test session that the test had been a success and commanded the astronauts to continue with the following test on the test plan. Figure 3.24 shows the magnitude of the error (Eq. 3.63) between the reference and actual trajectory in figure 3.23. The performance acquired is below the centimeter precision for most of the maneuver time. More precisely, the mean value of the magnitude error for this test was 5,1mm which is the best tracking error ever achieved for a circular maneuver in a SPHERES test session in the ISS.

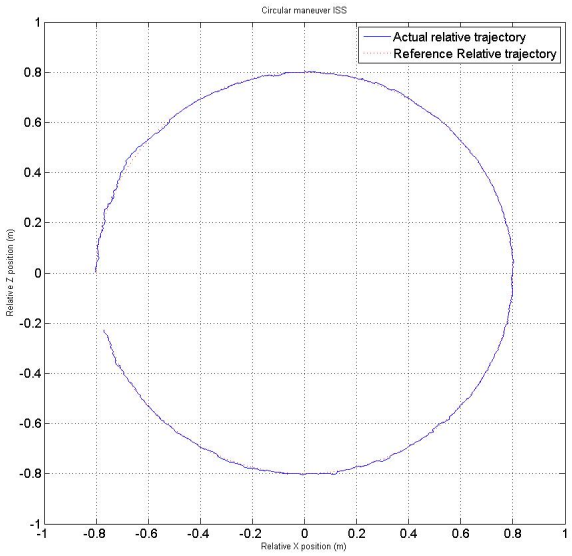

Figure 3.23: Circular maneuver, coupled dynamics control, ISS test

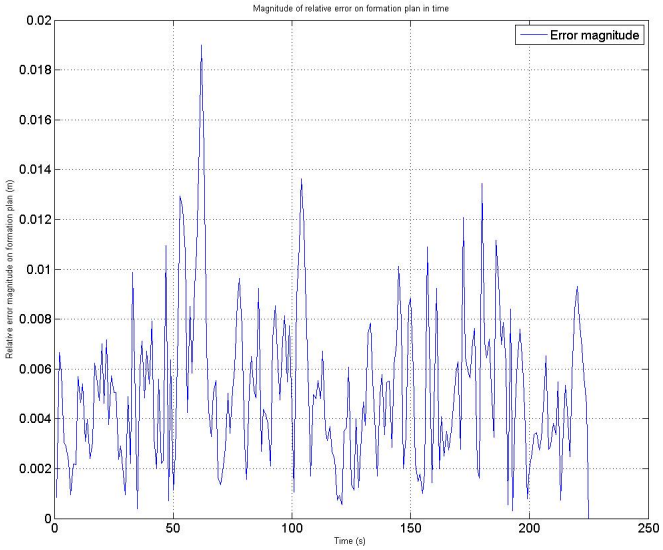

Figure 3.24: Magnitude of relative error on formation plan in time, coulpled dynamics, ISS test

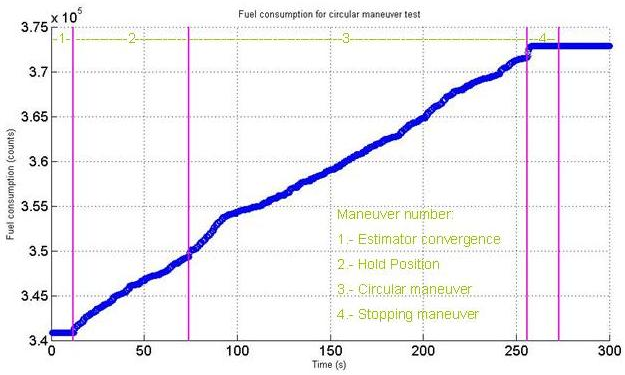

Figure 3.25: Fuel consumption of Sphere 2 for circular maneuver test

The other performance metric to be analyzed in this test is the fuel consumption, this being also part of the cost function that the optimal controller is supposed to minimize. As it has been already explained in the 3.7.1 section, the centroid control that requires the SPHERES testbed is detrimental to the fuel consumption with the coupled dynamics architecture. It is worth mentioning that the centroid control was expressly reduced –compared to the control effort for testing on the air table– before it was sent to the ISS due to the expected and known lower disturbing environment. However, the control effort was big enough to keep the centroid of the formation in the very center of the volume for the whole test preventing it from the desirable free-drifting centroid motion. This caused higher fuel consumption than the necessary. Let us illustrate this behavior with the image in figure 3.25 where the fuel consumption of one of the satellites is plotted in time.

As it can be seen in figure 3.25 the fuel consumption rate is roughly constant during the whole test. This means that the satellite was using the same amount of fuel just for holding position and for performing the circular maneuver. Thus, even if the control efforts were decreased before sending the algorithm to the ISS these were big enough to make the states oscillate into a very narrow deathband increasing the fuel consumption.

It must be noticed that this was the first test session where the coupled dynamics architecture was tested. Introducing the algorithm into the iterative process of testing on zero-gravity environment will lead to a better configuration of control efforts where

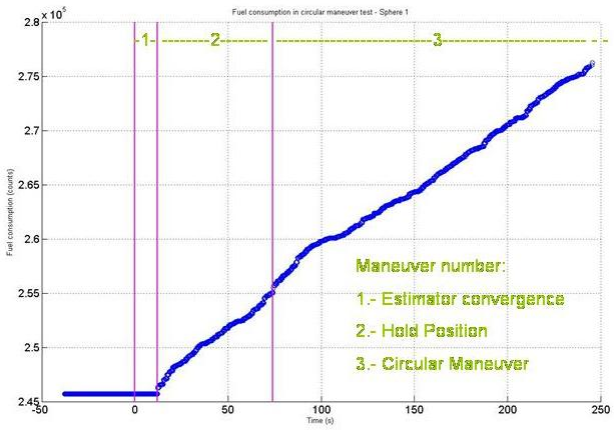

Figure 3.26: Fuel consumption of Sphere 1 for circular maneuver test

both high performances in tracking error and fuel consumption are achieved.

On the other hand, looking at the fuel consumption of the other satellite (figure 3.26), we can conclude that a balanced fuel consumption is achieved without the need of any additional control feature. The difference in fuel consumption within both satellites was below 3%.

Circular Maneuver test with independent and cyclic control

The following data was obtained from tests where satellites performed a circular maneuver in formation but a different architecture from the coupled dynamics one was used.

Figures 3.27, 3.28 and 3.29 represent a three satellite formation where each of them was independently commanded to follow a circular trajectory. While figure 3.27 shows a pretty accurate circular global trajectory of the satellites, figures 3.28 and 3.29 show that the precision in relative states is lower. Computing the mean value of the error magnitude plotted in figure 3.29 gives an average precision of 21,1mm.

The next architecture that has been used for comparison is the cyclic architecture. The cyclic pursuit algorithm [15] was used to perform a circular formation of three satellites. As it has been briefly mentioned at the beginning of this chapter, the cyclic pursuit algorithm has the intrinsic property of leading the satellites to converge to a circular moving formation of a specified radius. The algorithm uses to compute the

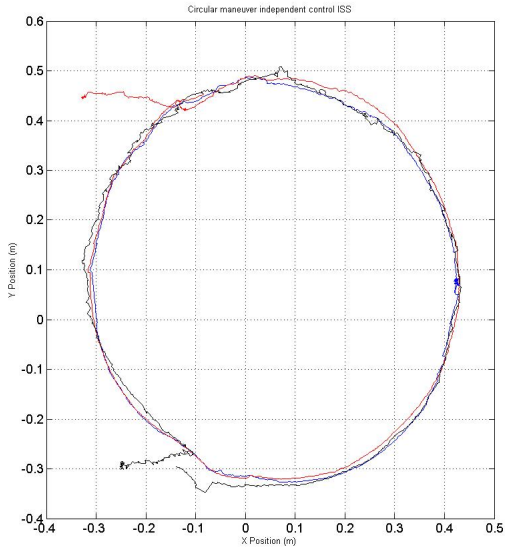

Figure 3.27: Circular maneuver with independent control, ISS test

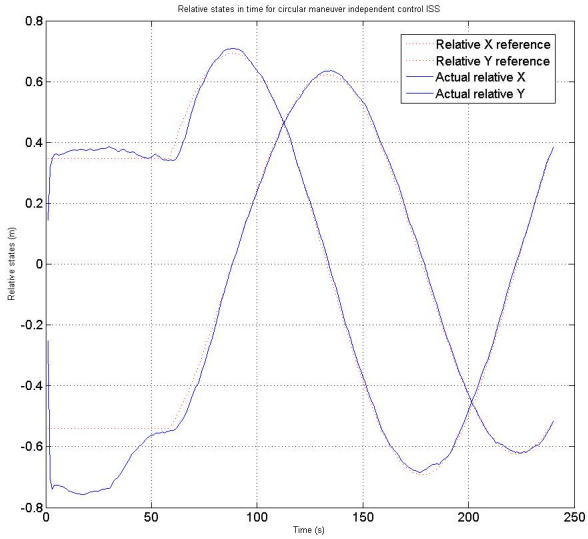

Figure 3.28: Relative position states in time for circular maneuver with independent control, ISS test

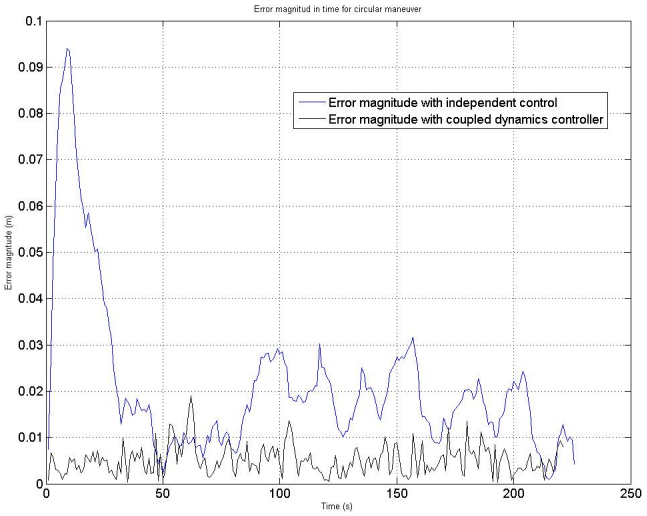

Figure 3.29: Magnitude of relative error on formation plan in time with independent control, ISS test

control commands the relative state to the satellite in front only. Nevertheless, it does not track any reference trajectory.

Figure 3.30 shows the effective circular global trajectory of the three satellites. Figure 3.31 shows the evolution of the relative states between two of the satellites which clearly corresponds to a circular evolution of the relative states. However, figure 3.32 shows that even if the relative states follow a circular motion satellites have not yet converged to the specified radius. The lack of a reference trajectory makes it senseless to estimate any tracking error here.

It is worth mentioning that even if the cyclic pursuit algorithm is not the most suitable one to track specific reference trajectories it does naturally converge to a circular formation and makes a very low fuel use for this purpose. At this point, the cyclic architecture is the one that used the less amount of fuel for completing one whole cycle. Specific values of fuel consumption for each of the architectures are displayed in the table at the end of this chapter.

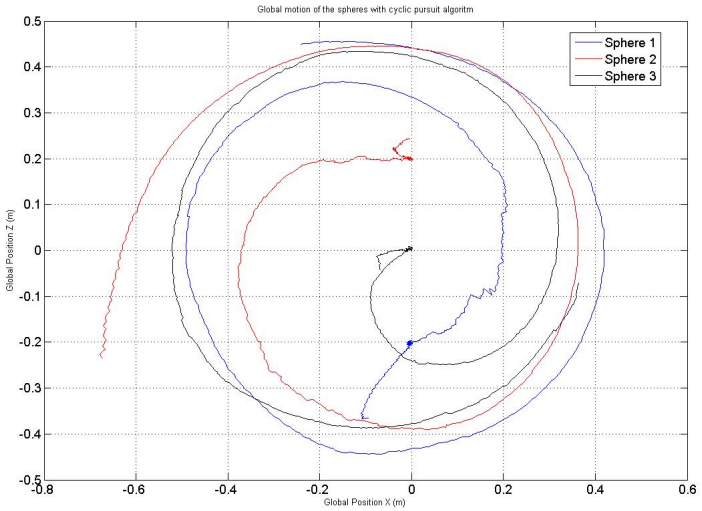

Figure 3.30: Global trajectory of Spheres with cyclic pursuit, ISS test

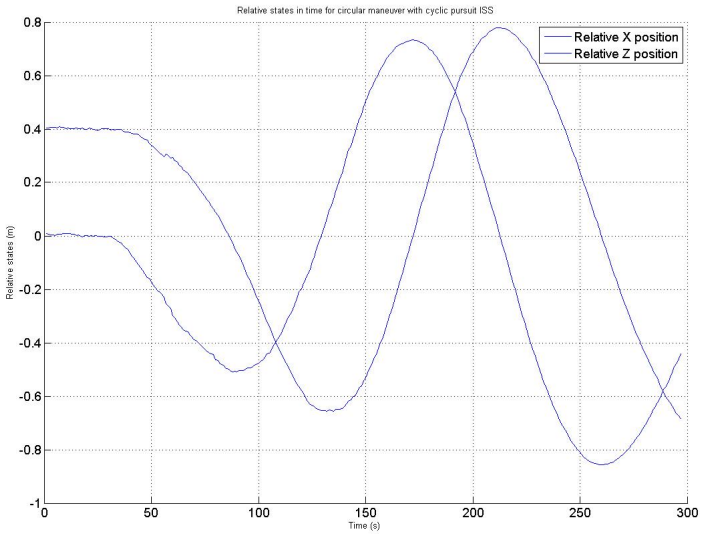

Figure 3.31: Relative position states in time for circular maneuver with cyclic pursuit, ISS test

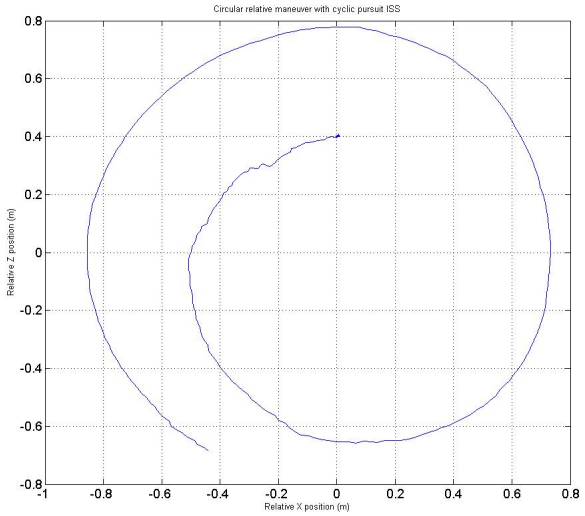

Figure 3.32: Circular relative trajectory with cyclic pursuit, ISS test

3.8.1.2 Spiral Maneuver

In the second test of the SPHERES 19th test session in the ISS where the coupled dynamics architecture was tested satellites performed a spiral maneuver. The test was very successful too, showing even better tracking performance than the circular maneuver test. Figure 3.35 shows that the relative trajectory plotted in figures 3.33 and 3.34 was tracked within millimeter precision for most of the maneuver. The mean value of the error magnitude for this maneuver was 4,5mm which makes it the most precise formation flight control test ever run in the ISS.

A very interesting event happened at the end of the maneuver when one of the satellites run out of gas and was unable to command any thruster firings for about the last 15 seconds of the maneuver. Even if the satellites where able to finish the maneuver it is clearly noticed that the tracking performance decreased significantly for that time. How the coupled dynamics architecture can deal with this and other inconvenient situations is treated in the 4th chapter of the thesis.

Spiral Maneuver test with independent control

The data showed in the following figures was obtained from a test where a two satellite formation performed a spiral maneuver using independent control and thus

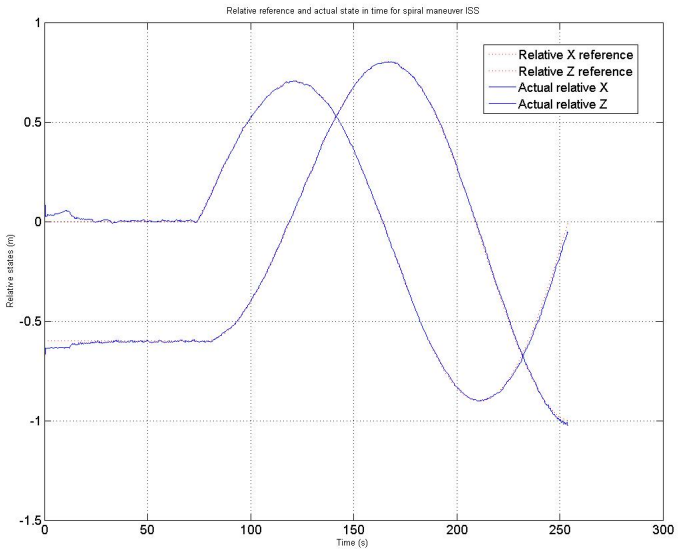

Figure 3.33: Relative position states in time for spiral maneuver with coupled dynamics, ISS test

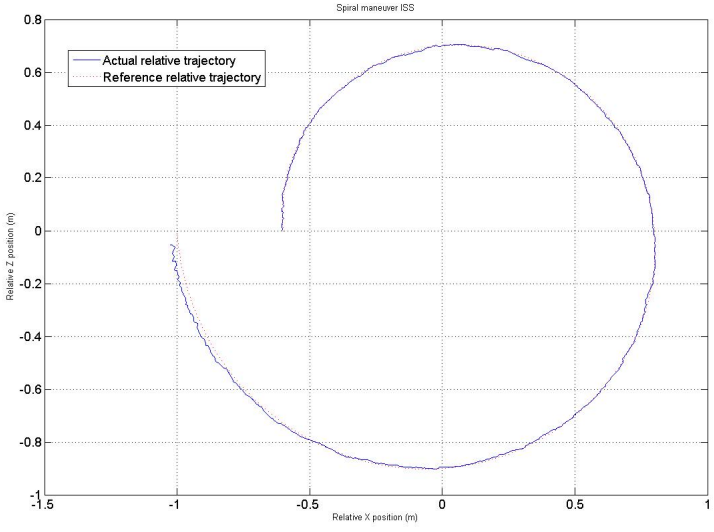

Figure 3.34: Spiral maneuver, coupled dynamics, ISS test

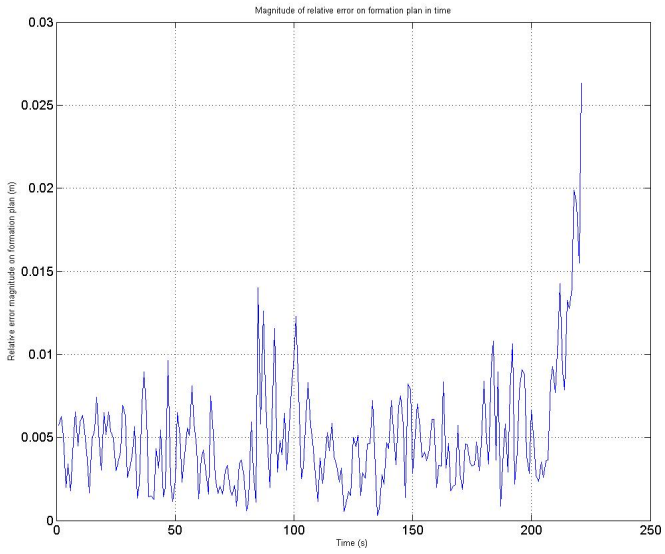

Figure 3.35: Magnitude of relative error on formation plan in time, ISS test

tracking two separate global trajectories. Even if the test was very successful with a global tracking mean error magnitude of 8mm and 7,5mm for each of the satellites, the precision goes down to 12,3mm when the error in relative states is computed. Figures 3.36 and 3.37 show the evolution of the relative states during the maneuver and the error magnitude of those.

3.8.1.3 Stop and Stare Maneuver

Finally, let us close this section mentioning that even if the Stop and Stare maneuver could not yet be run in the ISS at this point, the promising data from testing on the air table makes it expectable that successful data will also be obtained for this maneuver. Hopefully, this will help us concluding about the performance improvement that can be obtained when using the coupled dynamics architecture within these kind of interferometric maneuvers too.

3.8.2 Summary of testing in the ISS

Let us now regroup all the relevant data obtained from testing circular and spiral maneuvers in the ISS using different architectures.

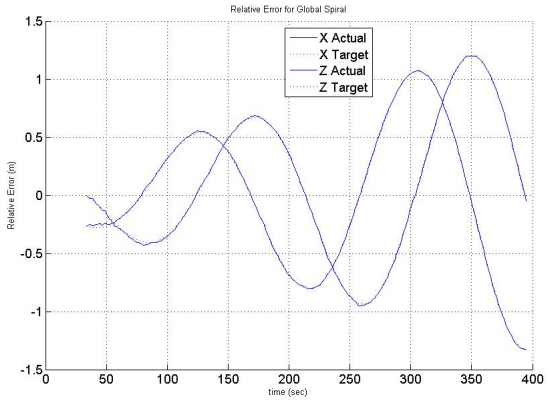

Figure 3.36: Relative position states in time for spiral maneuver with independent control, ISS test

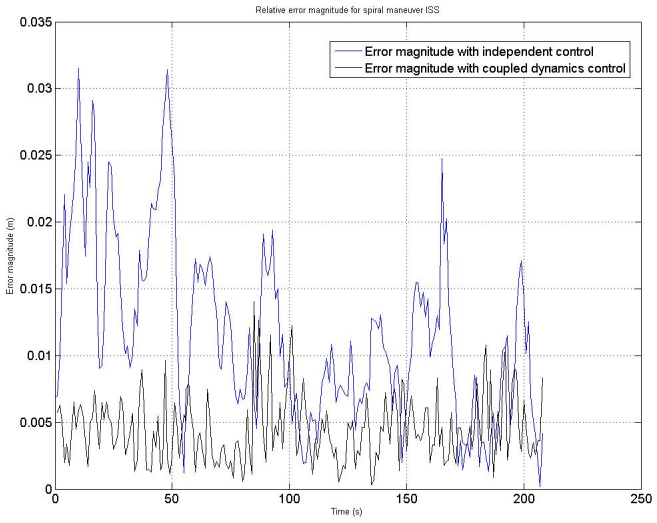

Figure 3.37: Magnitude of relative error on formation plan in time, ISS test

Maneuver	Architecture	Tracking error (mm)	Fuel use (g)
Circular	Coupled Dynamics	5,1	6,41
Circular	Independent	21,1	2,70
Circular	Cyclic	-	2,10
Spiral	Coupled Dynamics	4,5	7,01
Spiral	Independent	12,3	1,84

Table 3.8.1: ISS test results

It is worth mentioning that all the circular or spiral tests were performing similar or equal trajectories, this meaning same spinning rate and radius. This was expressly prepared so the performance metrics could be fairly compared.

3.9 Chapter Summary

In this chapter full design of formation flight controllers using the coupled dynamics architecture presented in chapter 2 was made. Controllers were implemented for testing the architecture in three different scenarios where they were compared to other formation flight controllers using different control architectures. The promising results obtained testing the controllers in the SPHERES air table were confirmed during the 19th SPHERES test session in the ISS when satellites performed the most precise formation flight control tests ever run.

On the other hand, the issue with the fuel use and the centroid control effort is willing to be mitigated in future SPHERES test sessions.

At the expectance of getting data from the next SPHERES test session where the coupled dynamics architecture will be tested in a Stop and Stare maneuver, those results will likely permit us conclude about the efficient fuel use that is made with the coupled dynamics architecture in formation flight maneuvers.

Chapter 4

Disadvantages of the coupled dynamics architecture

In the previous chapters, we have demonstrated how the coupled inter-spacecraft dynamics architecture can be used to design optimal formation flight controllers that show an improved performance in several interferometric maneuvers. In the present chapter we will focus on the disadvantages that using coupled dynamics reveals. Once the problematic is understood approaches to deal with them are presented. Those approaches are further implemented and tests in non nominal case scenarios are conducted in order to show the effects of several vagaries in the controller performance. Finally, the chapter ends with an evaluation of the ability of the adopted solutions to face those vagaries.

4.1 High information requirements

The global optimality of the coupled dynamics architecture is assured by taking into account the states of the whole formation at each control period and computing the control commands as a function of them. However, the number of relative states in a satellites formation grows as:

$$N_s \left(N_s - 1\right)/2 \tag{4.1}$$

where N_s is the number of satellites when only one direction for the relative vectors is considered. Each relative state needs to be measured by or communicated to each of the members of the fleet in order to compute by themselves the optimal control to apply at each loop. This is obviously an important requirement that increases the complexity of the system whether in communication or in sensing payload. Either there is a high communication requirement that translates in a lager allocated bandwidth or each of the satellites needs to be equipped with the required sensing payload. Any of both has as a consequence an increase in the economic cost of the system. Moreover, the main problem lies in the fact that the controller needs from those states in efforts to keep on computing the control commands. Not only the optimality of the controller is compromised but also, the more time the information takes to get to the satellites the more the controller risks to exceed the delay margin and thus destabilize the whole system.

For the tests results analyzed in chapter 3 a two satellite formation was considered. Therefore only one relative state was required by the controller. The communication bandwidth of the SPHERES testbed is big enough to guarantee with a high probability the reception of that required information by both satellites at each control loop, permitting the tests to be run in a nominal case without information loss.

However, if this algorithm were to be exported to another multi agent system with a higher number of members on the fleet the increasing information requirement could in fact become a deciding factor.

Next, how the coupled dynamics architecture can see the required information reduced without any loss of optimality will be explained. As a result, the required information will become increasing as a factor of N_s instead of N_s^2 as could be expected from equation 4.1. The technique will be added to the controller implementation and tests with a formation of three satellites will be run in the air table in non nominal case scenarios.

Let us consider the general case shown in figure 4.1 where a formation of three satellites is displayed.

As it can be seen in the picture, three relative states can be defined, named r_{12},

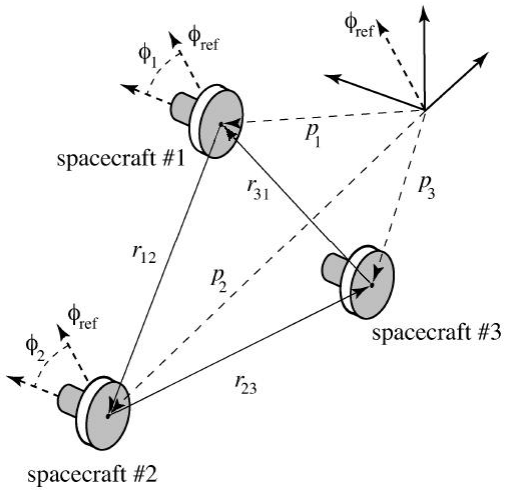

Figure 4.1: Example of satellite formation

r_{23} and r_{31} as formation states. Using the coupled dynamics architecture, a feedback control system could be implemented with the form:

$$\begin{bmatrix} u_1 \\ u_2 \\ u_3 \end{bmatrix} = \begin{bmatrix} K_{11} & K_{12} & K_{13} \\ K_{21} & K_{22} & K_{23} \\ K_{31} & K_{32} & K_{33} \end{bmatrix} \begin{bmatrix} r_{12} \\ r_{23} \\ r_{31} \end{bmatrix} \tag{4.2}$$

where relative velocity states where omitted for notational simplicity. However, if the formation states are well defined the next equations should always be satisfied:

$$r_{12} + r_{23} + r_{31} = 0 \tag{4.3}$$

We could then express one of the relative states as a linear function of the other two. In general, in a formation of N_s satellites only $N_s - 1$ out of the $N_s(N_s - 1)/2$ relative states are linearly independent. Thus, we can use a transformation matrix H in order to remove the unnecessary states and compute the control commands only by means of the $N_s - 1$ independent states.

$$\begin{bmatrix} u_1 \\ u_2 \\ u_3 \end{bmatrix} = KH \begin{bmatrix} r_{12} \\ r_{23} \\ r_{31} \end{bmatrix} = \begin{bmatrix} K_{11} + K_{12} & -K_{11} + K_{13} \\ K_{21} + K_{22} & -K_{21} + K_{23} \\ K_{31} + K_{32} & -K_{31} + K_{33} \end{bmatrix} \begin{bmatrix} r_{12} \\ r_{23} \end{bmatrix} \tag{4.4}$$

As it is proved in [37], such a controller that uses $N_s - 1$ measurements has same stability and performance properties as the one that uses all measurements $N_s(N_s - 1)/2$.

Not only we have considerably unloaded the high information requirements, but we also have shown that there exits several equivalent topologies (family of controllers) with same state tracking performances. In equation 4.4 state r_{31} was removed arbitrarily, but we could also decide to remove states r_{12} or r_{23} and the properties of the controller would remain the same. The possibility of switching from one topology to another gives robustness and redundancy to the system because if one of the state measurements suffers from communication link loss or sensing link loss –or just reveals a big noise level– then the system could decide to switch to another topology that is not using that precise state. Switching from one topology to another will just require of redefining the transformation matrix H but the rest of the controller design could stay invariant. As long as equation 4.3 is satisfied by the measured states then the control commands do not depend on the selected transformation matrix and switchings should occur without any visible effects in the performance of the controller.

In order to illustrate this fact with real data a test with a formation of three satellites was run on the SPHERES air table. Satellites followed a circular relative trajectory and they switched topologies at several points during the maneuver. Starting with all three relative states measured, they switched every 30 seconds to a different topology leading at the end of the maneuver to a situation where each of the satellites was using a different topology. This last situation could be given in the case of a communication blackout where each satellite needs therefore to sense the two relative vectors to the other two satellites. In figure 4.2 we can see the evolution in time of the tracking error to the relative states. Vertical lines indicate the moments during the test where a switching occurred.

As it was expected, no jumps in the tracking error are visibly due to any switching effect. This technique could then be applied to reduce the high information requirements and give redundancy to the system.

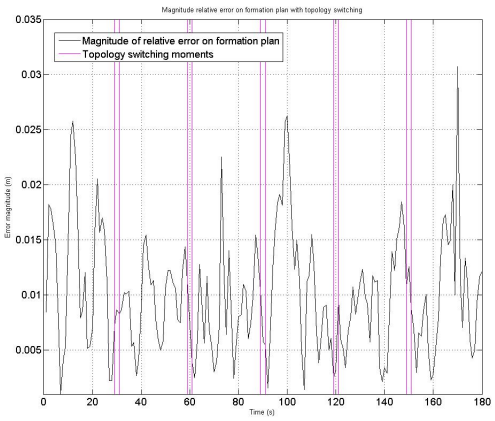

Figure 4.2: Evolution of magnitude of relative error in time with switching topologies, air table test

4.2 Low robustness to failure

Another disadvantage that appears when treating a multi agent system as a whole MIMO plant is that the failure of one satellite affects the performance of the whole formation. In other words, a local failure can have a global effect.

As it is shown in equation 4.2 the feedback control law returns the optimal commands for the actuators of each of the satellites. Then, the control system relies in every satellite executing the commanded controls. However, the fact that those commands could sometime not get executed by all satellites needs to be considered. That could be the case where one satellite would suffer from a thruster failure. Without actuators the satellite would drift freely and affect to the states of the whole formation. Moreover, the commands of the other satellites are not the optimal ones to track the relative states anymore.

At this point the decision of whether this satellite is kept as part of the formation or is declared failed needs to be made. If it is kept in the formation other satellites will try to track the relative states with a free drifting satellite which will decrease the performance and make the tracking error to rise. In case it is considered failed the rest of the flotilla should reconfigure to another formation where the relative states to the failed satellite are not considered in the controller anymore.

In the present research the author has studied the case where the underactuated

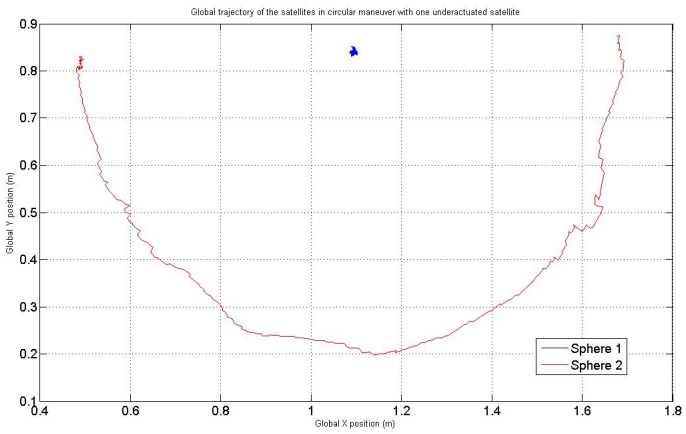

Figure 4.3: Global trajectory of Spheres in half circular maneuver with one underactuated satellite, air table test

satellite remains in the formation in a free drifting motion. The purpose of this case is to evaluate the performance worsening in these circumstances. A test with a two satellite formation was run in the SPHERES air table where only one of the satellites was actuating the control commands. The formation is commanded to perform a circular maneuver. Figure 4.3 shows the global trajectory followed by the satellites on the table. It can be seen that even if one of the satellites is just standing still on the table –simulated thruster failure– the other satellite is still able to perform the relative maneuver.

From the data obtained in this test and comparing it to the results presented in the previous chapter (section 3.7.2) it is concluded that the performance is indeed lower when one of the satellites presents a thruster failure; mean error magnitude for the latest maneuver is 2,4cm. However, it is worth considering that in this situation the total fuel used is much lower than in the nominal case. The total fuel use was reduced compared to the case where both satellites are firing in 45% due to the fact that the non actuated satellite does not spend any fuel but the actuated one requires a little bit more fuel to perform the maneuver on its own. This is an important result; it could be considered the case where instead of having two actuating satellites only one of them could be in charge of the relative control and achieve an acceptable relative tracking error while having a reduced fuel use. Moreover, we could find similarities

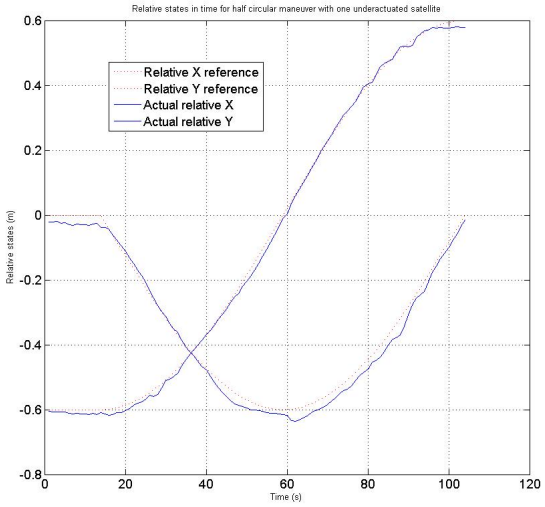

Figure 4.4: Relative position states in time for half circular maneuver with one underactuated satellite, air table test

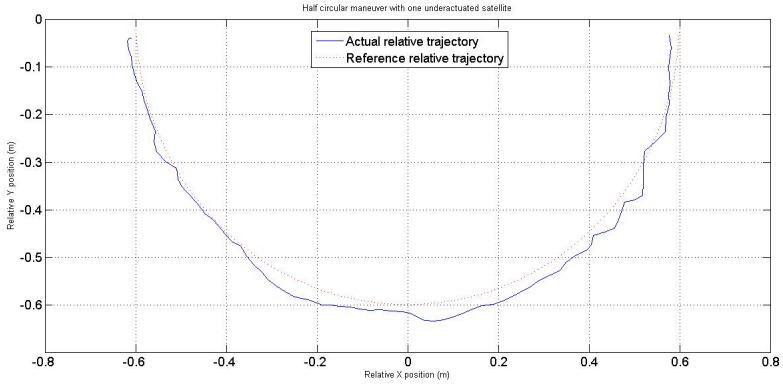

Figure 4.5: Relative trajectory in hal circular maneuver with one underactuated satellite, air table test

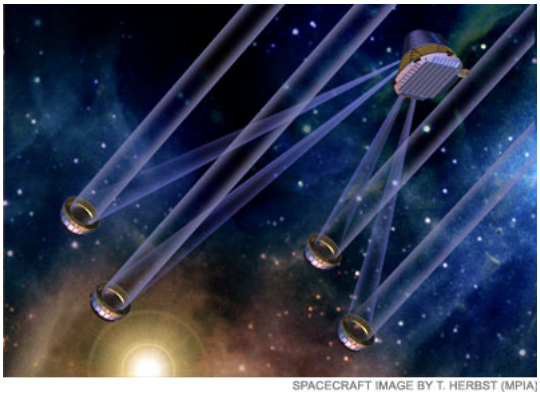

Figure 4.6: Art. representation of space interferometric formation flight mission [4]

of this case within future space interferometric formation flight missions where this algorithm could be applicable. Missions like Darwin [22], Terrestrial Planet Finder [25], Stellar Imager [9] and Planet Imager [20] for example are designed to be formed by several light-collectors and a one big combiner with the necessary payload to transmit all collected data to the Earth. In those cases, small satellites with fast dynamics (collectors) could be in charge of the relative control with respect to the combiner and unload the latest one from this task reducing the fuel to be boarded.

4.3 Chapter Summary

In this chapter the disadvantages that the coupled dynamics architecture presents have been discussed concluding that the main ones are the low robustness to local failures and the high information requirements. Techniques for dealing with these drawbacks have been developed and later implemented to test them in the SPHERES testbed. The data obtained from them was very useful and permitted in first instance showing how to reduce the information requirements by switching topologies. Secondly, the test that was run in non nominal conditions with an underactuated satellite, although it showed a lower performance, it opened the path to considering a slightly different control topology where the fuel use could be considerably reduced.

Finally, in the next chapter the global worthiness of the coupled dynamics architecture is discussed taking into account the advantages that have been proved, the

drawbacks that it presents and the techniques that we have to face the latest ones.

Chapter 5

Conclusions

5.1 Thesis summary and contributions

The necessity of further knowledge about the universe, its origins and new galaxies discovered requires improving the current imaging qualities of the observational space missions. Approaching the limit in angular resolution for monolithic space telescopes, a promising technology has emerged that would suppose an improvement without limits in image quality: the distributed telescope structure. The idea of translating the ground-based telescope array systems to the space supposes a fleet of satellites flying in formation where each of them works as a collector. Light coming from the same remote celestial source is then combined within the formation using interferometric techniques, which requires the system to perform very precise and stable relative configurations. The SPHERES testbed, built in the heart of the Space Systems Laboratory of MIT, permits the development and maturation of this challenging technology. The research in this thesis focuses on the design and implementation of a control system for a formation of satellites.

After addressing the importance of developing distributed spacecraft, the first part of this thesis deals with the problem of designing the control of a multi-agent system. An innovative approach is presented within a control architecture that defines coupled inter-spacecraft dynamics. The advantages that this architecture presents when applied to an interferometric formation flight space mission are discussed, concluding

in a performance improvement in trajectory tracking and reduced fuel use, the two most important factors that will determine the science output from an optical point of view and lifetime of a mission.

In the second part of this research, the architecture is tested in three different scenarios, picked for their importance in interferometric maneuvers. Optimal controllers for each of the scenarios are designed using the coupled dynamics architecture where a balance of the resources consumption and relative tracking error is minimized.

The successful results obtained from the first attempt to test the controllers in zero-gravity environment permit us to conclude that we can improve performance in tracking error when compared to controllers that are using other architectures. Results from further tests in zero-gravity will permit a more precise evaluation of reduced fuel use of the coupled dynamics architecture.

In the final section, the research focuses on the disadvantages that can be addressed when using the coupled dynamics architecture, including the high requirements in state information and the difficulties in robustness against local failures. Both of them are partially mitigated. The required information can be deduced by a technique that switches between topologies where the minimum information flow to compute the optimal control commands is adapted to the formation state and the available communication or sensing links. Secondly, the case of a local thruster failure was examined, which led to interesting results; a considerable amount of fuel is saved compared to the performance detriment in tracking trajectory. This test could open a new research path for the future where the underactuated satellite situation is also considered in the controller design.

This research contributes to the development and maturation process of control systems for formation flight spacecrafts. The coupled dynamics approach proved with data from testing in real space environment the performance improvement that can be achieved. A priori, the potential disadvantages of the architecture have been significantly overcome, making it a suitable and reliable approach. Thus, taking into account the demonstration of optimal performance, this could be a real step forward for the future of distributed telescope space missions.

5.2 Future work

Based on the research done and the knowledge acquired during this study the author proposes the following work for the future in order to keep on developing optimal controllers for formation flight spacecrafts.

The next logical step in further research should be testing the trajectory tracking controllers in the circular and spiral maneuvers with a reduced centroid control in order to evaluate the exact influence that this additional effort had in the use of fuel made in the latest tests in the ISS. The author believes that this will return very valuable data and expects it to provide conclusive information about the performance improvement that can be achieved both in fuel use and tracking accuracy.

At the same time, analyzing the data from testing the coupled dynamics architecture in a Stop and Stare maneuver in zero-gravity environment will provide important information that will help the evaluation of the architecture performance within this specific interferometric maneuver. A further step in the controller implementation for this kind of trajectory profile should be an additional feature that will help overcome the issue of the discrete time condition of the control system. This will consist on propagating (estimating) the states of the formation at each control period in order to anticipate the crossing of the switching curves on the phase-plane graph and thus reduce the possible overshoot that it could generate.

On the other hand, further research needs to be done to deal with the disadvantages of the architecture in order to increase the global robustness of the control system against significant loss of information. As the controller requires of a certain amount of information of the fleet in order to compute the optimal commands, a solution must be proposed for the unfavorable situations where this information is not available. The development of hybrid controllers is thought to be the next step forward to approach this problem.

Adding high level autonomous features would also be an interesting research that would increase the flexibility and reconfigurability of the formation enabling satellites to join or quit the formation depending on their state of health without the need of

a constant operating human supervision.

Finally, concerning the case of a numerous satellite formation system where the information requirements are more evident, different topologies should be studied where the information flow is relaxed by permitting a more decentralized suboptimal solution. Important work in this field is presented by Fax and Murray in [10] where the stability of different information topologies is discussed based on the Theory of Graphs and states the basis for the analysis of formation control stability.

Appendix A

Solving the optimal control problem

A.1 Matrix P(t) as solution of the Riccati equation

We are willing to prove in this section that the matrix P(t) relating the co-state and state variables in the LQ framework

$$\psi^*(t) = P(t)x^*(t) \tag{A.1}$$

is solution of the Riccati equation:

$$\dot{P}(t) = -P(t)A(t) - A^{\mathrm{T}}(t)P(t) - Q(t) + P(t)B(t)R^{-1}(t)B^{\mathrm{T}}(t)P(t) \tag{A.2}$$

We start taking derivatives at both sides of the equation A.1:

$$\dot{\psi}^*(t) = \dot{P}(t)x^*(t) + P(t)\dot{x}^*(t) \tag{A.3}$$

Given the necessary conditions:

$$\begin{aligned} \dot{x}(t) &= A(t)x(t) + B(t)u(t) \\ 0 = \tfrac{\partial}{\partial u}H &= R(t)u(t) + B^{\mathrm{T}}(t)\psi(t) \\ \dot{\psi}(t) &= -Q(t)x(t) - A^{\mathrm{T}}(t)\psi(t) \end{aligned} \tag{A.4}$$

We can rewrite equation A.3 introducing the information from the necessary conditions leading us to:

$$-Q(t)x(t) - A^{\mathrm{T}}(t)\psi(t) = \dot{P}(t)x(t) + P(t)\left(A(t)x(t) + B(t)u(t)\right) \tag{A.5}$$

Taking the expression of the optimal control law:

$$u^*(t) = -R^{-1}(t)B^{\mathrm{T}}(t)\psi^*(t) \tag{A.6}$$

and introducing it in A.4 and given A.1:

$$-Q(t)x(t) - A^{\mathrm{T}}(t)P(t)x(t) = \dot{P}(t)x(t) + P(t)\left(A(t)x(t) - B(t)R^{-1}(t)B^{\mathrm{T}}(t)P(t)x(t)\right) \tag{A.7}$$

which leads to the expression:

$$\left(-Q(t) - A^{\mathrm{T}}(t)P(t)\right)x(t) = \left(\dot{P}(t) + P(t)\left(A(t) - B(t)R^{-1}(t)B^{\mathrm{T}}(t)P(t)\right)\right)x(t) \tag{A.8}$$

and supossing $\exists t \diagup x(t) \neq 0$, then

$$-Q(t) - A^{\mathrm{T}}(t)P(t) = \dot{P}(t) + P(t)\left(A(t) - B(t)R^{-1}(t)B^{\mathrm{T}}(t)P(t)\right) \tag{A.9}$$

which is the expression that we wanted to demonstrate.

A.2 Expressions of the switching curves in the phase-plane graph for the optimal control solution in Stop and Stare maneuvers

In this section we will find the expressions of the curves on the phase-plane graph where the switching in between the different phases of the Stop and Stare maneuver occur. Given the Bang-off-Bang firing profile let us take the case where $u(t_f) = 2u_{max}$. Starting from the maneuver end corresponding to the origin of coordenates in phase-plane graph and integrating the commands, we got for the relative position state:

$$p_{rel}(t) = \frac{2u_{max}}{m}\frac{1}{2}t^2 + c_3 t + c_4 \quad for\ t \in (t_f - t_1, tf) \tag{A.10}$$

Given that at $t = t_f$,$p_{rel}(t)$ and $v_{rel}(t)$ are null:

$$c_3 = -\frac{2u_{max}}{m}t_f \quad and \quad c_4 = \frac{u_{max}}{m}t_f \tag{A.11}$$

and thus,

$$p_{rel}(t) = \frac{u_{max}}{m}(t - t_f)^2 \tag{A.12}$$

and since

$$v_{rel}(t) = \frac{2u_{max}}{m}t + c_3 = \frac{2u_{max}}{m}(t - t_f) \tag{A.13}$$

then the decelerating phase occur over the curve:

$$p_{rel}(t) = \frac{v_{rel}(t)^2}{\frac{4u_{max}}{m}} \tag{A.14}$$

which corresponds to the second switching curve in the maneuver. At $t = t_f - t_1$, where the coasting and the decelerating phases are switched:

$$p_{rel}(t_f - t_1) = \frac{m}{4u_{max}c_1^2} \tag{A.15}$$

and,

$$v_{rel}(t_f - t_1) = -\frac{1}{c_1} \tag{A.16}$$

During the coasting phase the velocity is constant and equal to the one at $t = t_f - t_1$, thus,

$$p_{rel}(t_1) - \frac{(t_f - 2t_1)}{c_1} = p_{rel}(t_f - t_1) = \frac{m}{4u_{max}c_1^2} \tag{A.17}$$

which gives that

$$p_{rel}(t_1) = \left(2\beta + \frac{m}{4u_{max}}\right)\frac{1}{c_1^2} \tag{A.18}$$

and taking equation A.16,

$$p_{rel}(t_1) = \left(2\beta + \frac{m}{4u_{max}}\right)v_{rel}^2(t_1) \tag{A.19}$$

so the first switching occurs along the curve:

$$p_{rel}(t) = \left(2\beta + \frac{m}{4u_{max}}\right)v_{rel}^2(t) \tag{A.20}$$

Let us now finish integrating the TPBP within the IC so that the expression for c_1 can be given. Studying the case of $v_{rel}(0) = 0$ and with $p_{rel}(0) = p_{rel0}$, the expression for the relative position during the accelerating phase is:

$$p_{rel}(t) = p_{rel0} - \frac{2u_{max}}{m}\frac{1}{2}t^2 \tag{A.21}$$

Matching the values of the relative position at $t = t_1$ that come from the accelerating phase (Eq. A.21) and the one coming from the coasting phase (Eq. A.18) we got:

$$p_{rel0} - \frac{2u_{max}}{m}\frac{1}{2}t_1^2 = \left(2\beta + \frac{m}{4u_{max}}\right)\frac{1}{c_1^2} \tag{A.22}$$

substituting the value of $t_1 = \frac{m}{2u_{max}c_1}$ already found leads to the final expression of c_1:

$$c_1^2 = \frac{\left(2\beta + \frac{m}{2u_{max}}\right)}{p_{rel0}} \tag{A.23}$$

Bibliography

[1] P. Nisenson A. Labeyrie, S.G. Lipson. *Optical Stellar Interferometry.* Cambridge University Press, 2006.

[2] et al Alvar Saenz-Otero. In *Distributed Satellite Systems Algorithm Maturation with SPHERES Aboard the ISS*, 59th International Astronautical Congress, Glasgow (Scotland), Sep-Oct 2008.

[3] Jacob G Katz Alvar Saenz-Otero and David W. Miller. In *SPHERES Demonstrations of Satellite Formations aboard the ISS*, AAS Guidance and Navigation Conference, Breckenridge, CO, Jan 30-Feb 4, 2009, Paper 09-011.

[4] Terrestrial Planet Finder artistic representation. Jet Propulsion Laboratory webpage: http://instrumentsystems.jpl.nasa.gov/projects/TPFI/.

[5] Dimitri P Bertsekas. In *Constrained optimization and lagrange multiplier methods*, New York : Academic Press 395 p.

[6] A. Saenz-Otero D. Miller Ch. Mandy, H. Sakamoto. In *Implementation of Satellite Formation Flight Algorithms Using SPHERES aboard the International Space Station*, International Symposium on Space Flight Dynamics, Annapolis, MD. September, 2007.

[7] S.R. Ploen D.P Scharf, F.Y. Hadaegh. In *A survey of spacecraft formation flying guidance and control (part 2): Control*, JPL Electronic Library. 2004.

[8] S.R. Ploen D.P Scharf, F.Y. Hadaegh. In *A survey of spacecraft formation flying guidance and control (part 1): Guidance*, Proceedings of the American Control Conference. June 4-6, 2003.

[9] K.G Carpenter et al. In *The Stellar Imager (SI): A revolutionary Large-Baseline Imaging Interferometer at the Sun-Earth L2 point*, NASA Goddard Space Flight Center. 2005.

[10] J. Alexander Fax and Richard M. Murray. In *Information Flow and Cooperative Control of Vehicle Formations*, IEEE TRANSACTIONS ON AUTOMATIC CONTROL, VOL. 49, NO. 9, SEPTEMBER 2004.

[11] S.A. Parvez G.Q. Xing and D. Folta. In *Design and implementation of synchronized autonomous orbit and attitude control for multiple spacecraft formation using GPS measurement feedback*, AAS/AIAA Spaceflight Mech. Mtg., pp. 115-134, 2000.

[12] V. Kapila H. Wang and A.G. Sparks. In *Adaptive output feedback tracking control of spacecraft formation*, Int. J Robust & Nonlinear Cont. vol. 12(2-3), pp. 117-139, 2002.

[13] M.O. Hilstad. In *A Multi-Vehicle Testbed and Interface Framework for the Development and Verification of Separated Spacecraft Control Algorithms*, M.S Thesis. Massachusetts Institute of Technology. May, 2002.

[14] Space Telescope Science Institute. In *General Overview of the Hubble Space Telescope*, http://www.stsci.edu/hst/.

[15] Emilio Frazzoli-David W. Miller Jaime Ramirez, Marco Pavone. In *Distributed Control of Spacecraft Formation via Cyclic Pursuit: Theory and Experiments*, American Control Conference, St Louis, MO, Jun 10-12, 2009, Paper FrB07.1.

[16] R.E. Kalman. In *Contributions to the Theory of Optimal Control*, Bol. Soc. Mat. Mex. (1960), 102-119.

[17] R.E. Kalman. In *The Theory of Optimal Control and the Calculus of Variations*, Mathematical Optimization Techniques, R. E. Bellman, ed. Santa Monica, Cal.: The RAND Corpotation, 1963.

[18] V. Kapila. In *Actuator Saturation Control*, KM Grigoriadis, 2002.

[19] D.E. Kirk. In *Optimal Control Theory: An Introduction*, Prentice Hall Inc. Englewood Clis. New Jersey, 1970.

[20] JET PROPULSION LABORATORY. In *Planet Imager*, http://origins.jpl.nasa.gov/missions/missions.html.

[21] P.L Falb M. Athans. In *Optimal Control*, Dover Publication Inc. Mc Graw Hill, 1966.

[22] A. Karlsson M. Fridlund, R. den Hartog. In *Scientifc Requirements on Space Interferometers*, JENAM2005 "Distant Worlds": Technology Roadmap for Future Interferometric Facilities. Liiege, Belgium. 4-7 July, 2005.

[23] G. Inalhan M. Tillerson and J.P. How. In *Co-ordination and control of distributed spacecraft systems using convex optimization techniques*, Int. J Robust & Nonlinear Control, vol. 12(2,3). pp. 207-242, 2002.

[24] L. Breger M. Tillerson and J.P. How. In *Distributed coordination and control of formation flying spacecraft*, Amer. Contr. Conf., pp. 1740-1645, 2003.

[25] K. Kroening E. Johnson M. Wehner, S. Moses. In *Terrestrial Planet Finder Space Vehicle Architecture Trades*, SPIE Conference on Astronomical Interferometry, Kona, Hawaii. March, 1998.

[26] Emilio Frazzoli Marco Pavone. In *Decentralized Policies for Geometric Pattern Formation and Path Coverage*, Journal of Dynamic Systems, Measurement, and Control SEPTEMBER 2007, Vol. 129 pp 633-643.

[27] A.G. Richards M.O. Hilstad, J.P. Enright. In *The SPHERES Guest Scientist Program*, Massachusetts Institute of Technology. Space Systems Laboratory. 2003.

[28] G. Yang M.S. de Queiroz, Q. Yan and V. Kapila. In *Global output feedback tracking control of spacecraft formation flying with parametric uncertainty*, IEEE Conf. on Decision and Control, pp. 584-589, 1999.

[29] S. Nolet. In *Development of a Guidance, Navigation and Control Architecture and Validation Process Enabling Autonomous Docking to a Tumbling Satellite*, PhD Thesis. Massachusetts Institute of Technology. June, 2007.

[30] F.Y. Hadaegh P.K.C. Wang and K. Lau. In *Synchronized formation rotation and attitude control of multiple free-flying spacecraft*, J Guid. Contr.& Dyn., vo l. 22(1), pp. 28-35, 1999.

[31] J. Ramirez S. Chakravorty. In *Fuel Optimal Maneuvers for Multispacecraft Interferometric Imaging Systems*, Journal of Guidance Control and Dynamics, Vol. 30 No. 1. January-February, 2007.

[32] A. Saenz-Otero. In *Appendix G Spheres Software Design*, M.S Thesis. Massachusetts Institute of Technology. June, 2005.

[33] A. Saenz-Otero. In *The SPHERES Satellite Formation Flight Testbed: Design and Initial Control*, M.S. Thesis. Massachusetts Institute of Techonology. August, 2000.

[34] A. Saenz-Otero. In *Design Principles for the Development of Space Technology Maturation Laboratories Aboard the International Space Station*, PhD Thesis. Massachusetts Institute of Techonology. June 2005.

[35] R.S. Smith and F.Y. Hadaegh. In *Control topologies for deep space formation flying spacecraft*, Amer Control Conf, pp. 2836-2841, 2002.

[36] R.S. Smith and F.Y. Hadaegh. In *Closed-Loop Dynamics of Cooperative Vehicle Formations With Parallel Estimators and Communication*, IEEE TRANSACTIONS ON AUTOMATIC CONTROL, VOL. 52, NO. 8, AUGUST 2007.

[37] R.S. Smith and F.Y. Hadaegh. In *Control Formation with Relative Sensing and switched information*, JOURNAL OF GUIDANCE, CONTROL, AND DYNAMICS Vol. 28, No. 1, JanuaryFebruary 2005.

[38] P.K.C. Wang. In *Navigation strategies for multiple autonomous mobile robots moving in formation*, J Robotic Syst. vol. 8(2), pp. 177-195, 1991.

[39] P.K.C. Wang and F.Y. Hadaegh. In *Coordination and control of multiple microspacecraft moving in formation*, J Astro. Scl., vol. 44(3), pp. 315-355, 1996.

[40] SPHERES ISS Data Base website. http://ssl.mit.edu/spheres/ISSdb/.

[41] K. Yamanaka. In *Simultaneous translation and rotation control law for formation flying satellites*, AIAA Guid. Nav. & Contr. Conf., 2000. AIAA Paper No. 2000-4440.